A Volcano Rekindled: The Renewed Eruption of Mount St. Helens, 2004–2006
Edited by David R. Sherrod, William E. Scott, and Peter H. Stauffer
U.S. Geological Survey Professional Paper 1750, 2008

Chapter 32

Chemistry, Mineralogy, and Petrology of Amphibole in Mount St. Helens 2004–2006 Dacite

By Carl R. Thornber[1], John S. Pallister[1], Heather A. Lowers[2], Michael C. Rowe[3], Charles W. Mandeville[4], and Gregory P. Meeker[2]

Abstract

Textural, compositional, and mineralogical data are reported and interpreted for a large population of clinoamphibole phenocrysts in 22 samples from the seven successive dacite spines erupted at Mount St. Helens between October 2004 and January 2006. Despite the uniformity in bulk composition of magma erupted since 2004, there is striking textural and compositional diversity among amphibole phenocrysts and crystal fragments that have grown from, partly dissolved in, or been accidentally incorporated in the new dacite. This study demonstrates that magma erupted throughout the current dome-building episode is the end product of small-scale, thorough mixing of multiple generations of crystal-laden magma. The mixed amphibole population provides important clues to magma conditions within the dacite magma reservoir prior to ascent and, to some extent, the dynamics of mixing and ascent.

The predominant amphibole in new dome rock ranges from moderate- to high-alumina tschermakite and magnesiohastingsite compositions. As substantiated by major- and trace-element geochemistry and barometry calculations, this compositional range of crystals, along with plagioclase, orthopyroxene, and iron-titanium oxide, is likely to have precipitated from dacite magma over a range of pressures and temperatures consistent with experimentally determined phase relations (~900°C to ~800°C between 100 MPa and ~350–400 MPa or ~4-km and 13.5–15-km depth). Along with trace-element characteristics, textural and compositional data help to distinguish some low-alumina magnesiohornblende crystals as xenocrysts. The diverse range in composition of amphibole in all samples of 2004–6 dacite, and the complex zonation observed in many phenocrysts, suggests a well-mixed source magma with components that are subjected to repeated heating and (or) pressurization within this pressure-temperature window. Amphibole textural and compositional diversity suggest dynamic conditions in the upper-reservoir zone, which has been tapped steadily during ~2 years of continuous and monotonous eruption. This well-mixed crystal mush is likely to have been subjected to repeated injection of hotter magma into cooler crystal-laden magma while simultaneously assimilating earlier generations of dacitic roof material and surrounding gabbroic rock.

Decompression-related reaction rims around subhedral, rounded, resorbed, and fragmented amphibole phenocrysts, regardless of composition, indicate that this mixed-crystal assemblage was being broken, abraded, and dissolved in the magma as a result of mechanical mixing before and during early stages of ascent from conduit roots extending into a mushy cupola of the shallow reservoir. In the earliest lava samples (October 2004), amphiboles with <3-μm rims associated with a glassier matrix than later samples suggest a slightly faster ascent rate consistent with the relatively high eruptive flux of the earliest phases of dome extrusion. Reaction rim widths of ~5 μm on amphibole in all subsequently extruded lava result from a steady influx and upward transport of magma from 3.5–2.5-km to ~1-km depth at rates of ~600 to ~1,200 m/day, through a conduit less than 10 m in radius. Slower ascent rates inferred from volumetric-flux and matrix-crystallization parameters are explained by a widening of the conduit to greater than 60 m radius within 1 km of the surface.

[1] U.S. Geological Survey, 1300 SE Cardinal Court, Vancouver, WA 98683

[2] U.S. Geological Survey, Box 25046, Denver Federal Center, Denver, CO 80225

[3] Department of Geosciences, 104 Wilkinson Hall, Oregon State University, Corvallis, OR 97331; now at Department of Geoscience, 121 Trowbridge Hall, University of Iowa, Iowa City, IA 52242

[4] American Museum of Natural History, Central Park West at 79th Street, New York, NY 10024

Introduction

The cooled and degassed dacite magma that has been tapped continuously by the 2004–6 eruption at Mount St. Helens is a mixture of 45 percent phenocrysts and 55 percent dacite melt (Pallister and others, this volume, chap. 30, table 4). As shown by Pallister and others (this volume, chap. 30), the whole-rock composition of lava erupted from 2004 to 2006 is strikingly uniform (64.9±0.09 weight percent SiO_2), and the dense-rock-equivalent (DRE) volume proportion of plagioclase (30–40 percent), amphibole (4–8 percent), orthopyroxene (3–5 percent), and iron-titanium-oxide (1–2 percent) phenocrysts is consistent throughout the eruption. Similarity of bulk-rock and bulk-matrix compositions, as well as the experimental phase equilibria of Rutherford and Devine (this volume, chap. 31), suggest that the dominant phenocryst assemblage shares a dacite parentage. However, the isotopic, mineralogical, and textural diversity of phenocrysts leaves little doubt that the bulk compositional uniformity is the end result of repeated and thorough mixing of phenocryst-laden magma with preexisting crystalline material.

Petrologic models of magmatic processes for this eruption rely, in part, upon mineral-melt criteria that are clouded by a genetically mixed population of phenocrysts. The phenocrysts, including variably resorbed, reacted, and fragmented crystals, are discrete pieces of a complicated "dacite puzzle." Some crystal populations look alike but did not necessarily crystallize together at the same depth, temperature, magma composition, and time. Detailed studies of phenocryst morphology and chemistry provide petrologic context for establishing the genetic affinities of the crystals. This chapter provides detailed documentation of the potpourri of amphibole phenocrysts in the 2004–6 lava at Mount St. Helens.

All amphibole found in 1980–86 and 2004–6 Mount St. Helens dome lava is calcium-rich, monoclinic amphibole (clinoamphibole). In fresh gray pieces of plagioclase-rich dacite (fig. 1), amphibole phenocrysts are conspicuous as dark-brown to black, lustrous to semitranslucent flecks, chunks, and, locally, flow-aligned acicular blades.

The ubiquitous amphibole phase in 1980–86 and 2004–6 Mount St. Helens dome rock incorporates all of the major-element components of a water-saturated dacite melt and, thus, records changes in the pressure-temperature (*P-T*) paths and the compositional variations of host magmas at depths in excess of ~ 4 km, where amphibole is stable (~100 MPa, Rutherford and Devine, this volume, chap. 31). Clinoamphibole phenocrysts dissolve in magmas undergoing decompression and degassing during ascent. The nature and extent of amphibole breakdown reactions record the rates and paths of magma ascent from depth (Rutherford and Hill, 1993; Browne and Gardner, 2006; Buckley and others, 2006). In this study of newly erupted Mount St. Helens lava, we establish and correlate variations in texture, chemistry, and mineralogy among amphibole crystals, and we document and interpret the characteristics of amphibole reaction rims. Aluminum-in-amphibole thermobarometry is applied to infer the relative *P-T* conditions for the range of amphiboles likely to have crystallized from host dacite or similar magma. We aim to provide an

Figure 1. Photograph showing freshly broken surface of SH325-1A, a typical sample of Mount St. Helens 2004–6 dacite lava.

"amphibolic" perspective toward understanding the character and disposition of a well-mixed, cooled, and degassed magma beneath Mount St. Helens during its near-steady-state transport to the surface from 2004 to 2006.

Samples Used in this Study

This investigation is based on microbeam studies of 22 Mount St. Helens dacite samples erupted during the October 2004 to January 2006 interval of spine emergence and dome growth (table 1). Aside from the samples derived unequivocally from newly extruded material (including the March 8, 2005, ash-fall sample, MSH05DRS3/8-4), the suite described here includes two unusual glassy dacite fragments (SH300-1A3, SH304-2G) dredged from debris shed by the emergent dome in early October 2004. Because these two samples are of uncertain origin and are uniquely glassy, their data, along with data for lithic inclusions of nonjuvenile andesite and dacite found in lava samples SH315-4, SH325-1A, and SH321-1, are discussed separately. Petrologic attributes of several samples reported here are also reviewed elsewhere in this volume; for example, the petrology of the early glassy fragment (SH-04-2G) and the small, glassy andesite inclusion in SH315-4 are discussed by Pallister and others (this volume, chap. 30). An overview and complete catalog of samples collected during the 2004–6 eruption, including sampling methods, locations, brief descriptions, and chemistry, is presented for dome samples by Thornber and others (2008) and for tephra samples by Rowe and others (2008).

Three older dome samples from the Cascades Volcano Observatory (CVO) archive were also analyzed to assess differences between clinoamphibole chemistry from the current eruption suite and the 1980–86 dacite (table 1). Compositional data on amphiboles in two gabbro xenoliths from the 1986 dome rock (791-8a, 791-8b samples of Pallister and others, 1991) provide a basis for identifying xenolith-derived crystal fragments among the diverse population of amphiboles in the 2004–6 dacite.

Overview of Amphibole Data

Amphiboles in polished thin sections were selected for analysis without bias to size or morphology. Microbeam analyses and imagery used in this study were accomplished at three different laboratories (details of microbeam methods are in appendix 1). All amphibole analyses used in this investigation fit the mineralogical criteria established for calcic amphiboles by Leake and others (1997). The stoichiometric calculation used to assess cation site occupancy and proper nomenclature is discussed in a separate section below. Compositional data acquired include 458 major-element analyses of 399 individual crystals with 373 interior and 85 outer (20 μm) rim analyses. These data include 26 analyses of 17 crystals in lithic inclusions of andesite or dacite and 49 analyses of 28 crystals in glassy lithic samples. In addition, rare-earth elements were analyzed for 80 amphibole cores in nine samples spanning the 2004–6 eruption. No amphibole trace-element data are currently available for 1980–86 lava or xenolithic inclusions. All chemical analyses of 2004–6 amphibole phenocrysts compiled for this investigation are tabulated in appendix 2, which appears only in the digital versions of this work (in the DVD that accompanies the printed volume and online at http://pubs.usgs.gov/pp/1750). For purposes of the comparison with current eruptive products, major-element analyses of amphibole in 1980–86 Mount St. Helens dacite and in gabbroic xenoliths in the 1980–86 dome material also were compiled and are provided in appendix 2.

Maximum length and width measurements of 391 (98 percent) of the analyzed phenocrysts were made using scaled scanning electron microscope (SEM) images. Although providing a general assessment of amphibole crystal sizes and aspect ratios, this method does not consider variations resulting from crystal orientation within the plane of the thin section. Measurements of the average width of amphibole-breakdown rims resulting from decompression (Rutherford and Hill, 1993; Browne and Gardner, 2006) were made on 195 crystals having rims in contact with the 2004–6 dacite matrix. Care was taken to exclude any anomalous rim widths for crystals sectioned unevenly along their outer edges.

Amphibole Morphology and Reaction Textures

In typical new-dome material, amphibole grains range in size from phenocrysts <4 mm long to microphenocrysts ranging from 100 to 10 μm. An amphibole size distribution based upon approximate surface areas (length-by-width measurements) shows that nearly all of the smallest crystals observed ($<1\times10^3$ μm^2) are fragments with broken or irregular edges and that the amphibole population as a whole is more normally distributed about a range of $10–100\times10^3$ μm^2 (fig. 2). Distinctly resorbed edges are observed among broken and unbroken crystals. A 62-percent majority of the amphibole phenocryst population is equant to slightly acicular (0–10 percent acicularity) and 23 percent is distinctly acicular, with length/width ratios ranging from 2.5:1 to 5:1 (20–30 percent acicularity, fig. 3).

Morphologic variants of isolated amphibole grains in 2004–6 dacite-lava samples include (1) subhedral, equant to acicular crystals with well-defined faces and typically, but not always, multiple, compositionally distinct growth zones (fig. 4); (2) angular fragments, variably rounded or embayed and commonly broken along cleavage planes that intersect normal growth zones (fig. 5); (3) well-rounded and seemingly abraded grains lacking substantially embayed or cuspate grain boundaries (fig. 6); and (4) irregularly shaped, rounded and embayed crystals or crystal fragments, commonly with fine

Table 1. Summary of Mount St. Helens 2004–2006 samples used in this investigation.

Sample No.	Spine No.	Collection date	Eruption date[1]	Sample type	Rock type
SH100		9/8/1981	9/6/1981	Dome talus	Dacite
SH133		6/5/1985	2/1–3/31/1983	Dome rock	Dacite
SH187		6/6/1989	5/30/1985	Dome rock	Dacite
SH300-1A3	1	10/20/2004	10/15/2004	Crater debris, either 1985 or Oct 2004 (?)	Dense dark-gray glassy dacite fragment
SH300-1C	1	10/20/2004	10/15/2004	Crater debris, either 1985 or Oct 2004 (?)	Vesicular dark-gray dacite fragment
SH302-1A	1 or 2	10/27/2004	10/14/2004	Crater debris, either1985 or Oct 2004 (?)	Vesicular dark-gray dacite fragment
SH304-2A	3	11/4/2004	10/18/2004	Dome talus and debris	Vesicular “hot-pink” dacite
SH304-2G	3	11/4/2004	10/18/2004	Dome talus and debris	Dense dark-gray glassy dacite fragment
SH305-1	3	1/3/2005	11/20/2004	Spine margin	Vesicular gray dacite
SH306-A	4	1/14/2005	12/15/2004	Dome talus	Vesicular pink-gray dacite
SH308-3	4	2/22/2005	1/21/2005	Dome talus	Vesicular gray dacite
SH309-1C	4	2/22/2005	1/13/2005	Spine margin	Vesicular gray-pink dacite, fractured foliated
SH311-1B	4	1/19/2005	1/16/2005	Ballistic block, 1/16/2005 explosion	Vesicular gray dacite
MSH05DRS_3_9_4	4	3/9/2005	3/8/2005	Coarse fragments in tephra-fall deposit from 3/8/2005 explosion	Vesicular gray-pink dacite
SH312-1	4	4/10/2005	3/8/2005	Ballistic block, 3/8/2005 explosion	Vesicular gray dacite
SH314-1A1	5	4/19/2005	4/17/2005	Gouge fragment	Vesicular dacite fragment
SH315-3	4	4/19/2005	4/1/2005	Dome talus, 4/18/2005 collapse	Dense gray dacite
SH315-4	4	4/19/2005	4/1/2005	Dome talus, 4/18/2005 collapse	Dense gray dacite
SH317-4	5	6/15/2005	5/1/2005	Dome talus	Dense pink-gray dacite
SH319-1	5	7/13/2005	5/15/2005	Dome talus	Dense gray-pink dacite, foliated, “pink” margins
SH321-1	6	8/19/2005	8/10/2005	Dome talus, 8/19/2005 collapse	Dense gray-pink dacite, “pink” margins
SH323-2, -3	6	10/18/2005	9/10/2005	Dome talus, 8/19/2005 collapse	Dense gray dacite
SH324-1A	7	12/15/2005	12/5/2005	Spine margin	Vesicular gray-pink dacite
SH324-3	7	12/15/2005	12/5/2005	Spine margin	Dense gray dacite
SH325-1	7	2/7/2006	12/20/2005	Dome talus	Dense gray dacite

[1] Estimate of when sampled lava was extruded from vent, whose altitude is assumed to be that of the crated floor below Crater Glacier.

to coarse cuspate margins indicative of magmatic resorption (fig. 7). The patterns of compositional zoning apparent in SEM backscattered electron images of many crystals or fragments typically define subparallel growth bands. In numerous cases, regardless of grain morphology, zoning patterns have an irregular or patchy appearance. This characteristic has been attributed to late-stage igneous (near-solidus) diffusion (Hammarstrom and Zen, 1992) but could result from patchy dissolution and regrowth (M.J. Rutherford, written commun., 2006).

Many amphibole crystals or fragments in the new Mount St. Helens dacite have glass inclusions (fig. 4) or partially to wholly crystallized melt inclusions (glass±opx±plg±oxides;

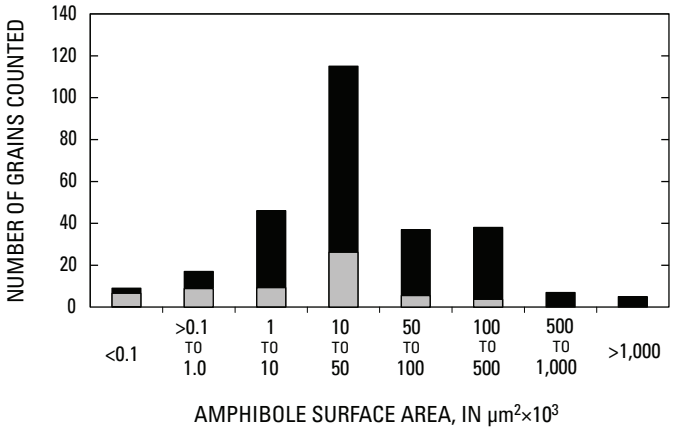

Figure 2. Histogram of size distribution of amphibole phenocrysts in Mount St. Helens 2004–6 dacite lava presented as approximate surface area. The size distribution of fragmented crystals, shown in gray, is compared to that of the overall population, shown in black.

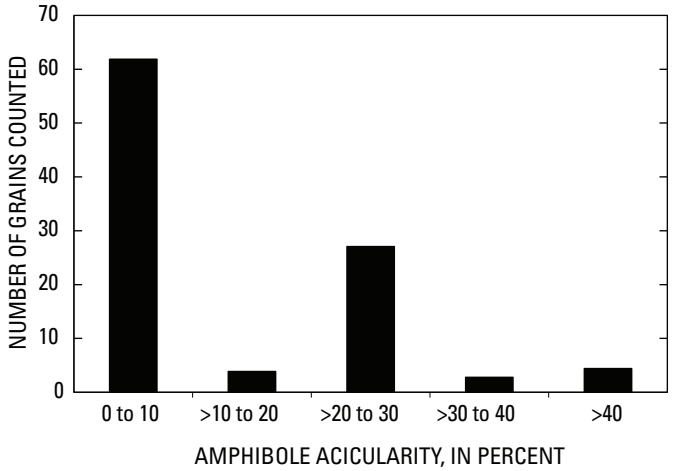

Figure 3. Histogram of acicularity of amphibole phenocrysts in Mount St. Helens 2004–6 dacite lava. Percent acicularity = [100 × length/(length + width)] – 50. (Equant crystals have zero-percent acicularity).

for example, fig. 5*B*), suggestive of variable cooling or reaction rates among a mixed phenocryst population. Amphibole phenocrysts of subhedral and resorbed morphology also are present in glomerophyric clusters, coupled during growth with various combinations of plagioclase, orthopyroxene, or oxide crystals (fig. 8). Although some of the more pristine-looking glomerophyric aggregates appear as though they grew in the dacite host, those cored by resorbed amphiboles may have resulted from prolonged amphibole-melt reaction, as discussed further below.

Because of similarities in texture and degree of reaction, there might be no definitive textural distinction between cognate and xenocrystic aggregates, such as those derived from gabbroic xenolith fragmentation. The latter could appear relatively pristine (unreacted or unresorbed) if exposed to the degassed host melt during xenolith fragmentation at near-solidus temperatures and shallow depths.

The edges of all amphibole crystals in contact with matrix in 2004–6 dacite lava are armored by an aureole of acicular microlites of plagioclase and orthopyroxene (±Fe-Ti oxide). As demonstrated by experiments, such rims result from reaction of clinoamphibole with dacite melt during decompression and degassing (Rutherford and Hill, 1993; Browne and Gardner, 2006). Rim widths are a function of the rate and path of ascent of the host magma during transport to the surface from a minimum P_{H_2O} of 100 MPa where amphibole is stable (>3.5–4 km depth at Mount St. Helens).

Essentially all of the amphibole crystals measured have decompression reaction rims between 3 and 8 μm thick; average reaction-rim width is 5±1 μm. Typical reaction rims pseudomorphically replace the outer edges of subhedral, rounded, or resorbed crystals and fragments (fig. 9). Exceptions to the normal reaction-rim thickness are observed in the earliest dome sample (SH304-2A, fig. 9*B*), which has <3-μm-thick rims, and the glassy lithic fragment (SH304-2G, fig. 9*A*), in which amphibole crystals lack reaction rims. Atypically thick rims (30–200 μm) are found among isolated amphibole crystals in 2004–6 dacite. These rims are defined by relatively coarse-grained plagioclase-orthopyroxene-oxide intergrowths that surround embayed (resorbed) amphibole grains (fig. 10).

An unusual but recurrent texture observed in SH314-1 and DRS_3_9_4 indicates amphibole reacting with the host melt to form second-generation amphibole + liquid (fig. 11). Such amphibole-to-amphibole reaction reflects exposure to a hotter or chemically incompatible melt under amphibole saturation conditions. As discussed further within the context of the compositions of these crystals, this amphibole-to-amphibole reaction is likely to occur at depths near the low-pressure limits of amphibole stability (100 MPa).

Amphibole phenocrysts in lithic inclusions (SH315-4inc, SH325-1Ainc, and SH321-1inc) have reaction-rim characteristics that differ from those of the host 2004–6 dacite. The SH315-4 glass-bearing inclusion has distinctly acicular amphibole intergrown with plagioclase and minor clinopyroxene, and it has an andesitic bulk composition (Pallister and others,

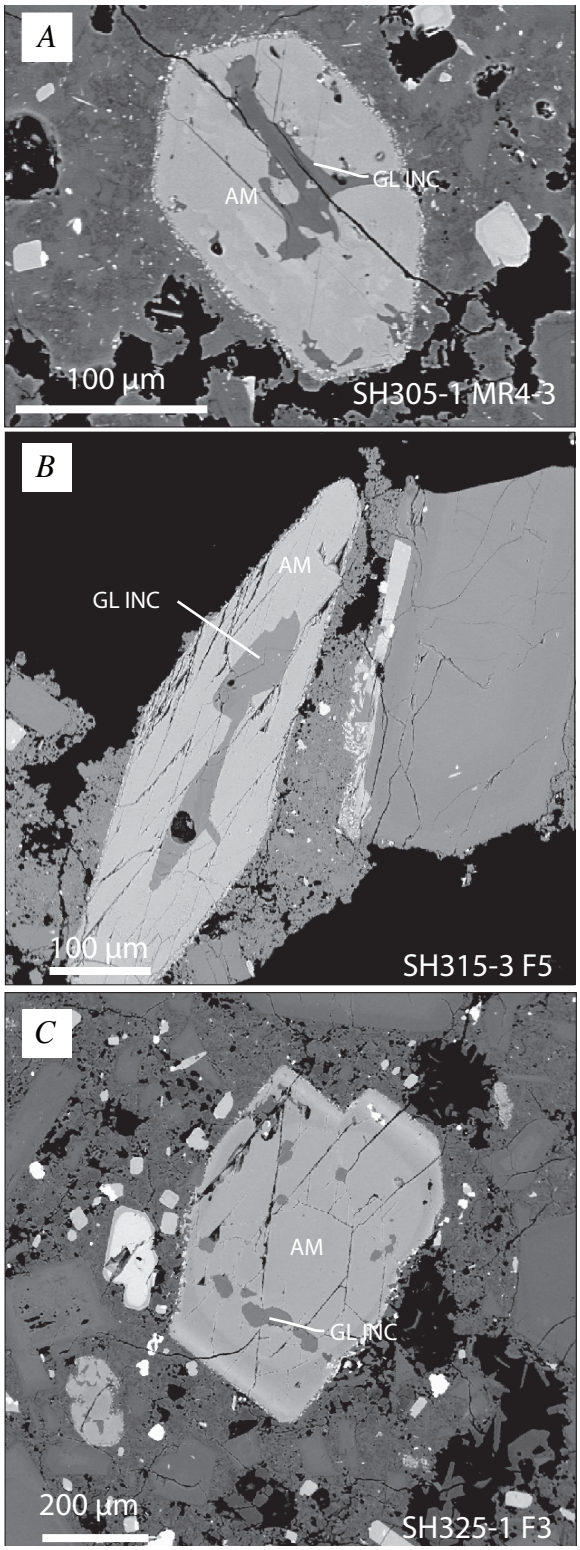

Figure 4. SEM backscattered electron images of analyzed subhedral amphibole grains (AM) in Mount St. Helens 2004–6 dacite lava. Glass inclusions (GL INC) indicated where confirmed by microbeam analysis. The sample and image numbers shown on the lower right side in each image correspond to analysis numbers in appendix 2. *A*, Sample SH305-1. *B*, Sample SH315-3. *C*, Sample SH325-1.

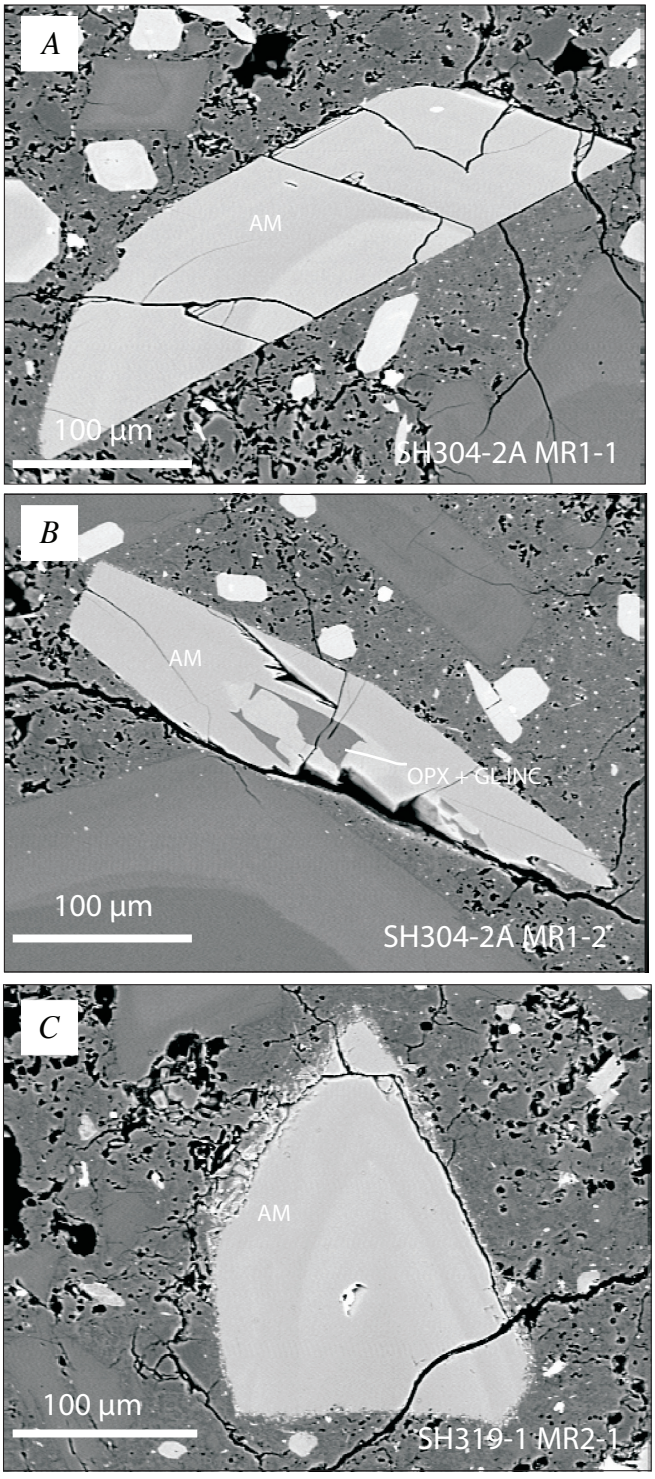

Figure 5. SEM backscattered electron images of analyzed broken amphibole grains (AM) in Mount St. Helens 2004–6 dacite lava. Orthopyroxene and glass inclusions (OPX + GL INC) are indicated where confirmed by microbeam analysis. The sample and image numbers shown on the lower right side in each image correspond to analysis numbers in appendix 2. *A*, Sample SH304-2A. *B*, Sample SH304-2A. *C*, Sample SH319-1.

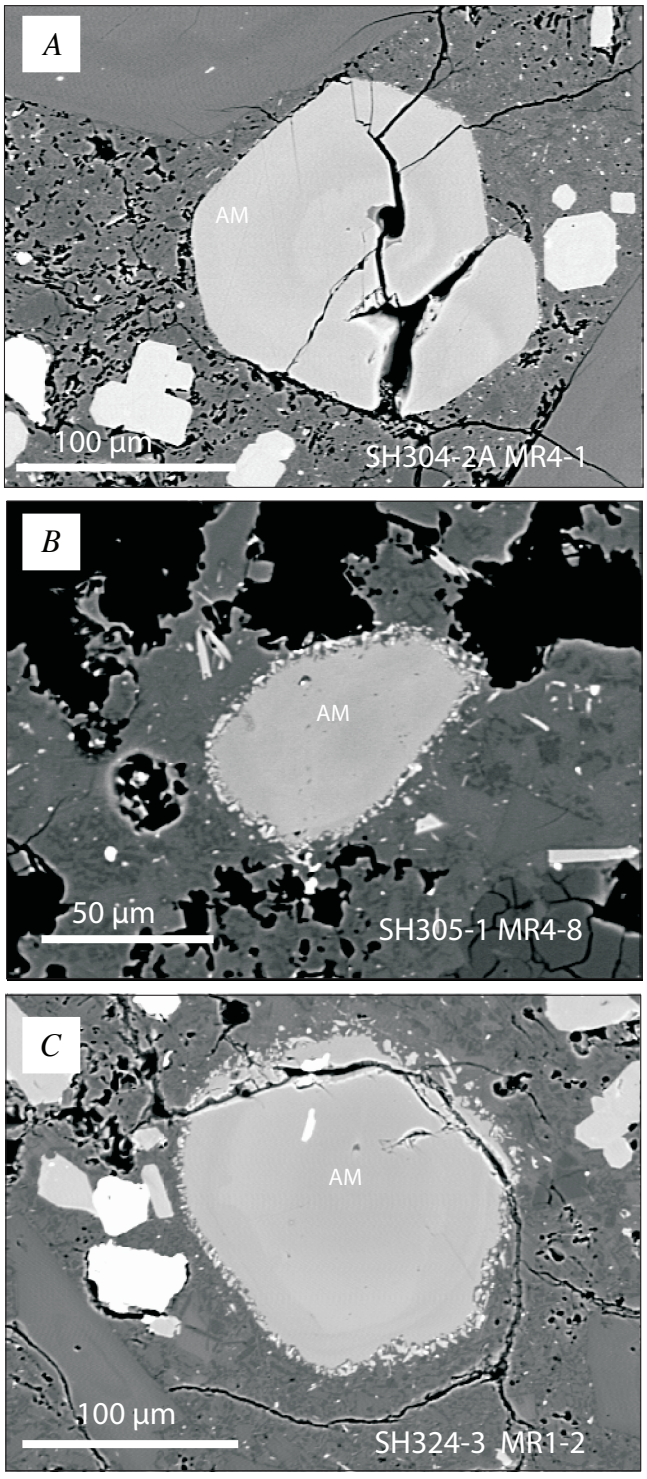

Figure 6. SEM backscattered electron images of analyzed rounded or abraded amphibole grains (AM) in Mount St. Helens 2004–6 dacite lava. The sample and image numbers shown on the lower right side in each image correspond to analysis numbers in appendix 2. *A*, Sample SH304-2A. *B*, Sample SH305-1. *C*, Sample SH324-3.

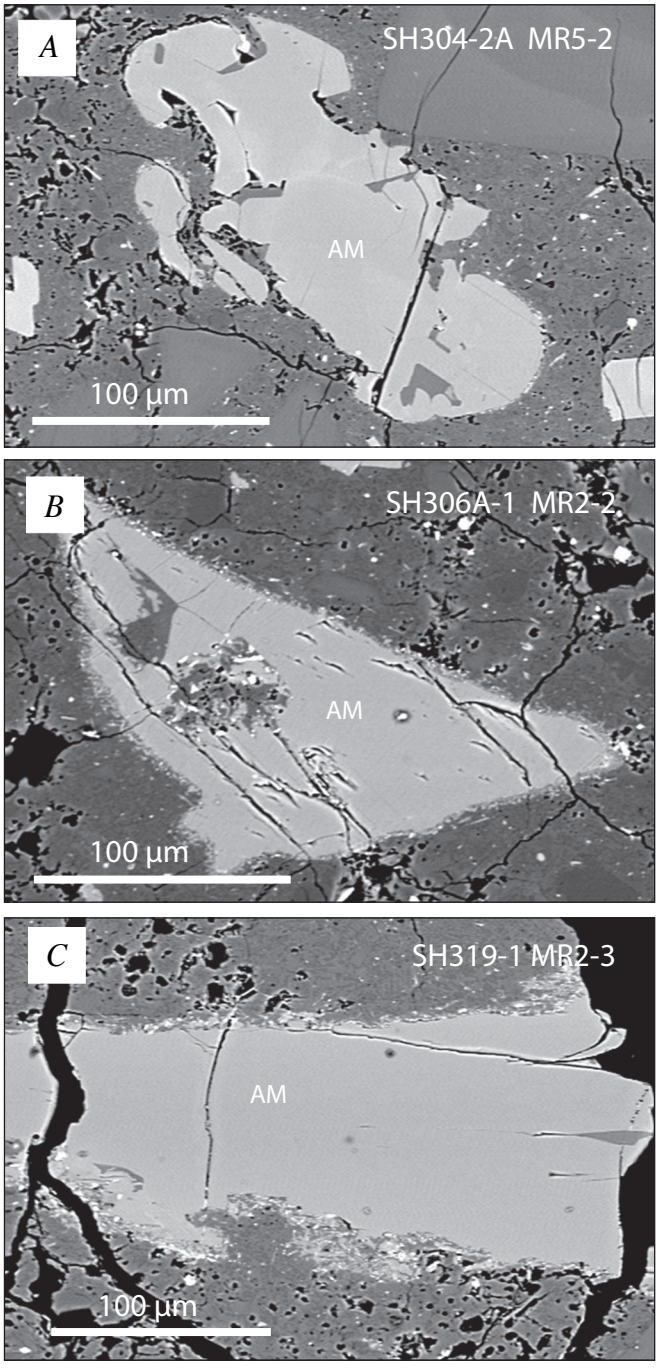

Figure 7. SEM backscattered electron images of resorbed amphibole crystals (AM) with embayed and cuspate margins in Mount St. Helens 2004–6 dacite lava. The sample and image numbers shown on the upper right side in each image correspond to analysis numbers in appendix 2. *A*, Sample SH304-2A. *B*, Sample SH306A-1. *C*, Sample SH319-1.

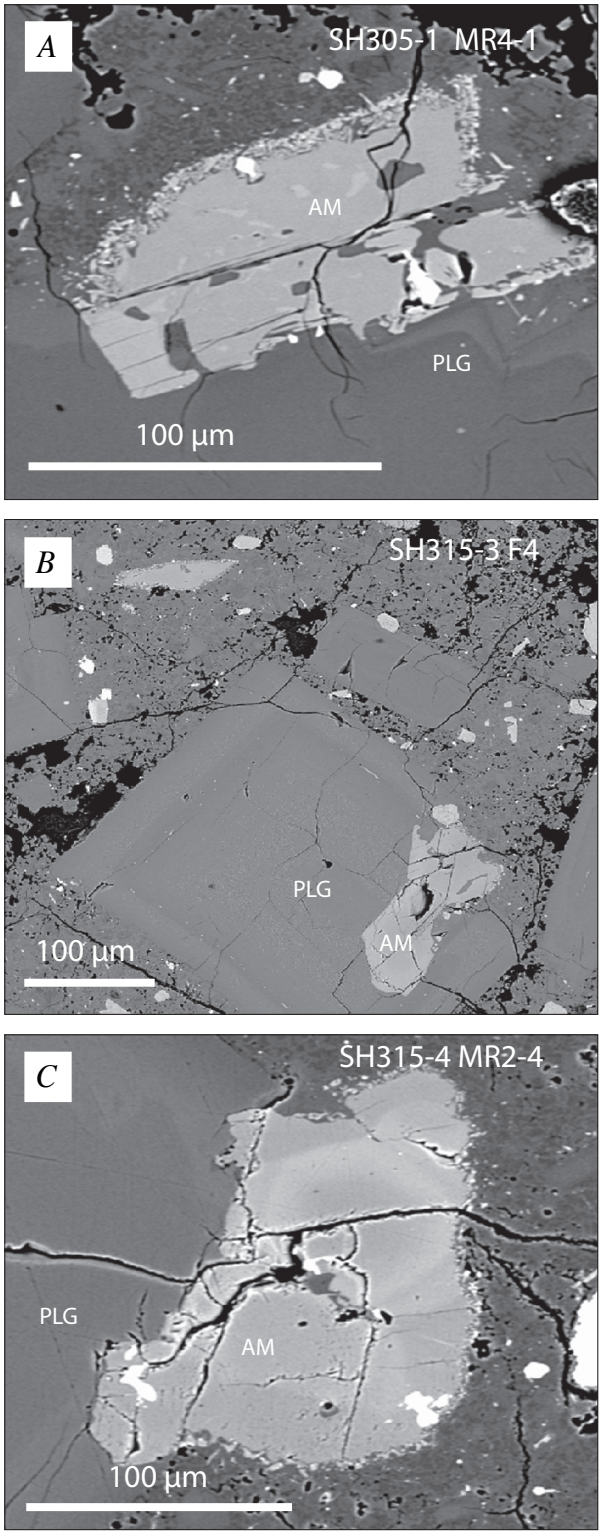

Figure 8. SEM backscattered electron images of amphibole grains (AM) intergrown with plagioclase (PLG) in Mount St. Helens 2004–6 dacite lava. The sample and image numbers shown on the upper right side in each image correspond to analysis numbers in appendix 2. *A*, Sample SH305-1. *B*, Sample SH315-3. *C*, Sample SH315-4.

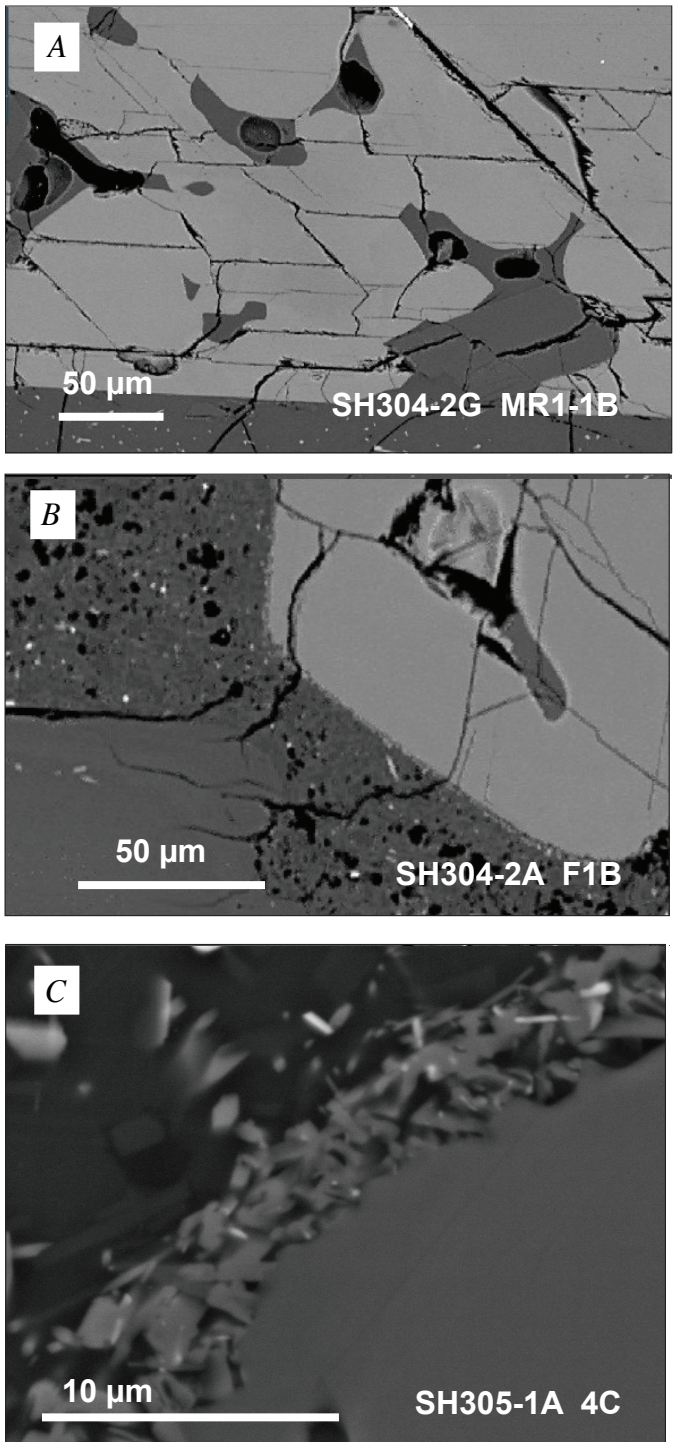

Figure 9. SEM backscattered electron images showing reaction rims around amphibole phenocrysts in Mount St. Helens 2004–6 dacite lava. The sample and image numbers shown on the lower right side in each image correspond to analysis numbers in appendix 2. *A*, No reaction rims present on amphiboles in glassy lithic fragment, SH304-2G. *B*, Rim widths are ~3 µm in October 2004 spine lava, SH304-2A. *C*, Typical 5-µm rims in all subsequent 2004–6 spine samples (SH305-1 shown here) are composed of an acicular microcrystalline intergrowth of plagioclase (dark colored), orthopyroxene (lighter colored), and Fe-Ti oxide (white).

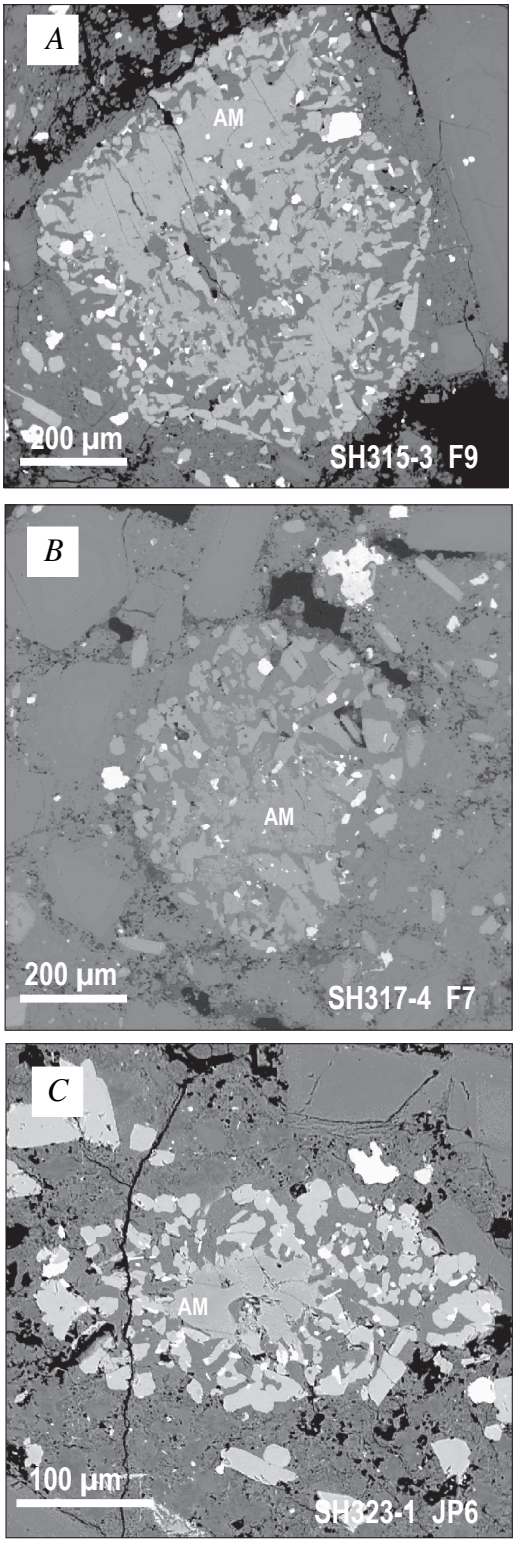

Figure 10. SEM backscattered electron images showing rare coarse-grained reaction rims (plagioclase + orthopyroxene + Fe-Ti oxide) around amphibole phenocryst remnants (AM) in Mount St. Helens 2004–6 dacite lava. The sample and image numbers shown on the lower right side in each image correspond to analysis numbers in appendix 2. *A*, Sample SH315-3. *B*, Sample SH317-4. *C*, Sample SH323-1.

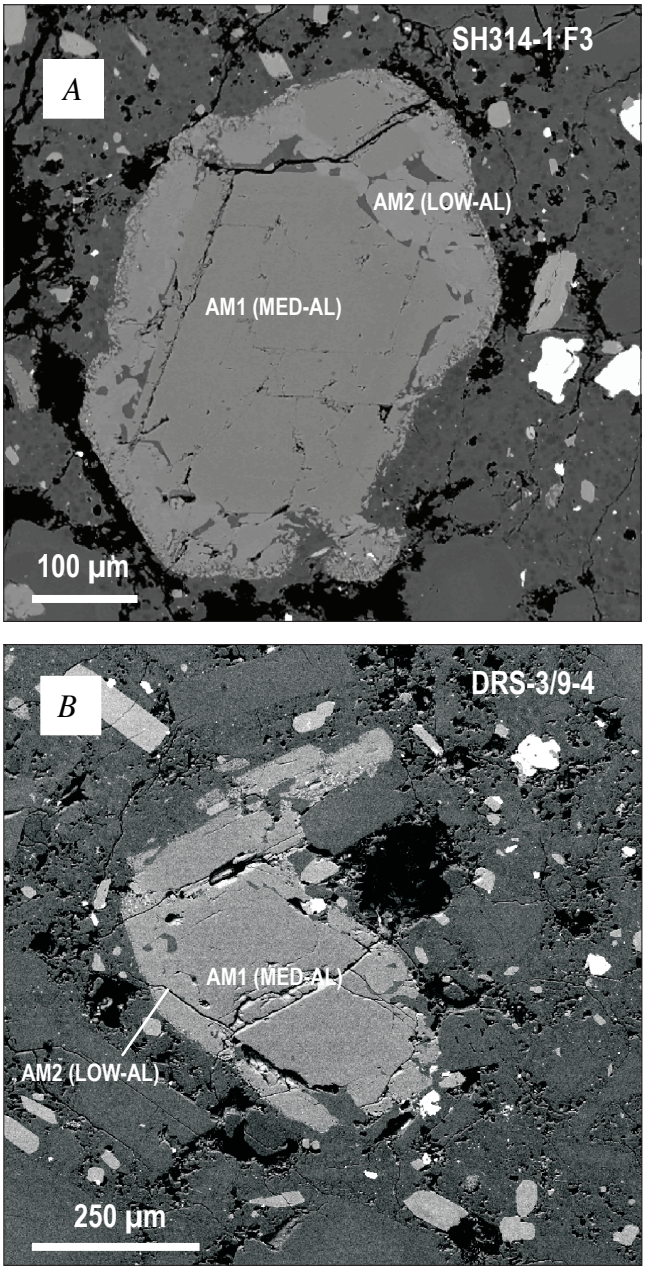

Figure 11. SEM backscattered electron images showing examples of amphibole-to-amphibole+melt reaction in Mount St. Helens 2004–6 dacite lava. The sample and image numbers shown on the upper right side in each image correspond to analysis numbers in table 2 and appendix 2. *A*, In sample SH314-1, amphibole with ~12.5 percent Al_2O_3 (AM1) is surrounded by aggregate of amphibole crystals (AM2) with ~7.2 percent Al_2O_3 and high fluorine (~0.18 percent) and glass (dark gray). *B*, In sample DRS_3_9_4, amphibole with ~12.2 percent Al_2O_3 (AM1) is surrounded by an aggregate of amphibole crystals (AM2) with ~6.9 percent Al_2O_3 and high fluorine (~0.25 percent) and glass (dark gray).

this volume, chap. 30). Reaction rims ~5-μm wide are found on the inclusion edge, where amphibole crystals are in contact with the dacite matrix, but no such rims occur along interior contacts between amphibole and glass. Inclusion SH325-1Ainc has a bulk texture similar to that of SH315-4inc, but the matrix lacks a significant glass component. Reaction rims are similarly restricted to grains in contact with the host dacite. These are the only andesite inclusions found among the well-scrutinized suite of 2004–6 dacite samples. They are small (<1.5 cm) and are likely accidental fragments derived from conduit walls. We do not consider them evidence of mafic-magma mixing.

Dacite inclusions such as SH321-1inc contain resorbed amphibole crystals with broad reaction rims similar to those found in the bimodal population in 1980–86 dacite (Rutherford and Hill, 1993; Cashman and McConnell, 2005). This inclusion also is distinguished from the 2004–6 host lava by the presence of clinopyroxene microphenocrysts in the matrix around amphibole, which is suggestive of isobaric heating of a cooler crystal-laden magma or of slow decompression of a newer hotter one (see Rutherford and Devine, this volume, chap. 31, fig. 10). It is theoretically possible that such fragments could have originated from eruption-related magmatic processes. However, like the andesite inclusions, these rounded fragments are more likely to be inconsequential xenoliths eroded from the shallow conduit walls.

We discern some fundamental characteristics of the 2004–6 dacite magma from the textures of its amphibole phenocrysts. The well-dispersed population of texturally diverse amphibole described above is a strong indication that the uniform composition of the dacite is inherited from a process of small-scale mingling and intermixing of crystal-laden magmas at depth. The consistent presence of variably zoned, broken, abraded, and resorbed amphibole crystals suggests that a number of temporally (and spatially) distinct crystallization environments are represented. Because similar 5-μm reaction rims are observed around all morphologic variants of amphibole, crystal fragmentation, abrasion, and resorption must have occurred at depth after assembly of the diverse crystal population and during initial stages of decompression with upward transport. Further discussion of amphibole-melt reaction textures and implications for dynamics of magma ascent is presented later in this chapter.

In the following sections, the chemistry and mineralogy of this textural medley of amphibole phenocrysts are reviewed to ascertain genetic distinctions and to gain insight into magmatic conditions associated with the 2004–6 eruption.

Amphibole Major-Element Chemistry

Amphibole phenocrysts analyzed to date in 2004–6 Mount St. Helens dacite (fig. 12; table 2; appendix 2) are all clinoamphibole with a calcium content of ~11.0 weight percent (11.0±0.3 percent CaO). Their silica and alumina contents span a continuous range that varies inversely between average end members with high silica and low alumina (47.5 percent SiO_2, 6.4 percent Al_2O_3) and low silica and high alumina (41.8 percent SiO_2, 15.0 percent Al_2O_3) (fig. 13*A*). The prevalent

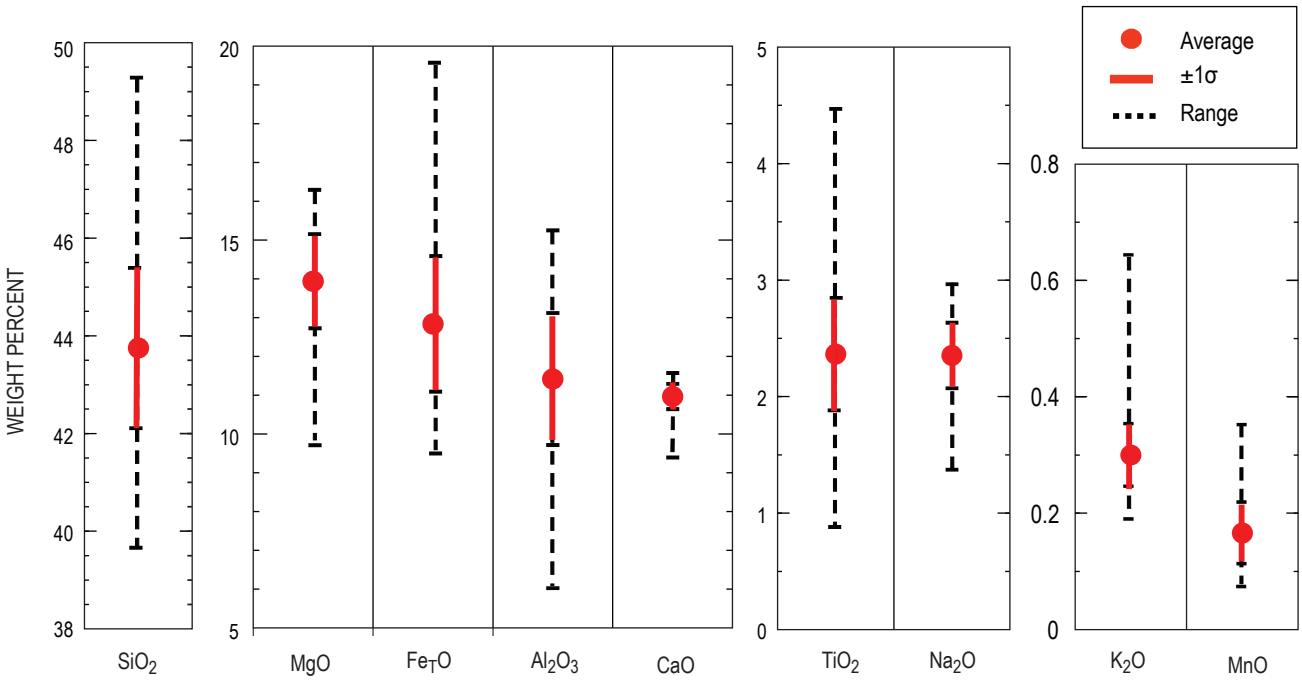

Figure 12. Average, range, and standard deviation of major elements analyzed in Mount St. Helens 2004–6 amphibole phenocrysts (excluding data from crystals in lithic inclusions and glassy lithic fragments). Fe_TO is all iron calculated as Fe^{2+}.

2004–6 amphibole compositional range, defined as ±1σ variation from the mean, is from 42.1 to 43.8 percent SiO_2 and 11.4 to 9.7 percent Al_2O_3.

Three compositional trends are evident within the silica/alumina range of amphibole crystals in dome dacite (and dome-derived ash) by the patterns of Mg and Fe variation with Al (figs. 13*B*, 13*C*). The low-alumina range (low-Al), from 6 to ~9 percent Al_2O_3, has a sympathetic increase in Fe_TO (all iron calculated as Fe^{2+}) averaging from 12 to 15.5 percent associated with decreasing MgO from 16 to 12 percent. Over the mid-alumina range (medium-Al), from ~9 to 12 percent Al_2O_3, average Fe_TO decreases to 12 percent and MgO increases to 12–16 percent. High-alumina (high-Al) amphibole ranges from ~12 to 15 percent Al_2O_3, with a corresponding average Fe_TO increase to 16 percent and a MgO decrease to ~11 percent.

Amphibole phenocrysts of high-Al, medium-Al, and low-Al compositions are present and distributed similarly in nearly all 2004–6 samples examined, as well as in 1980–86 dacite samples (fig. 14*A*). Our data reveal that amphibole in 2004–6 and 1980–86 dacites have the same range of major-element compositions. The low-Al amphiboles in old and new dacite overlap the phenocryst compositions in gabbroic xenoliths (fig. 14*A*). Amphibole crystals in the SH304-2G glassy lithic fragment are chiefly medium-Al in composition but display a low- to high-Al range similar to that of the 2004–6 population (fig. 14*B*). The high-Al amphibole compositions of lithic inclusions (SH315-4inc and SH325-1Ainc) are similar to those

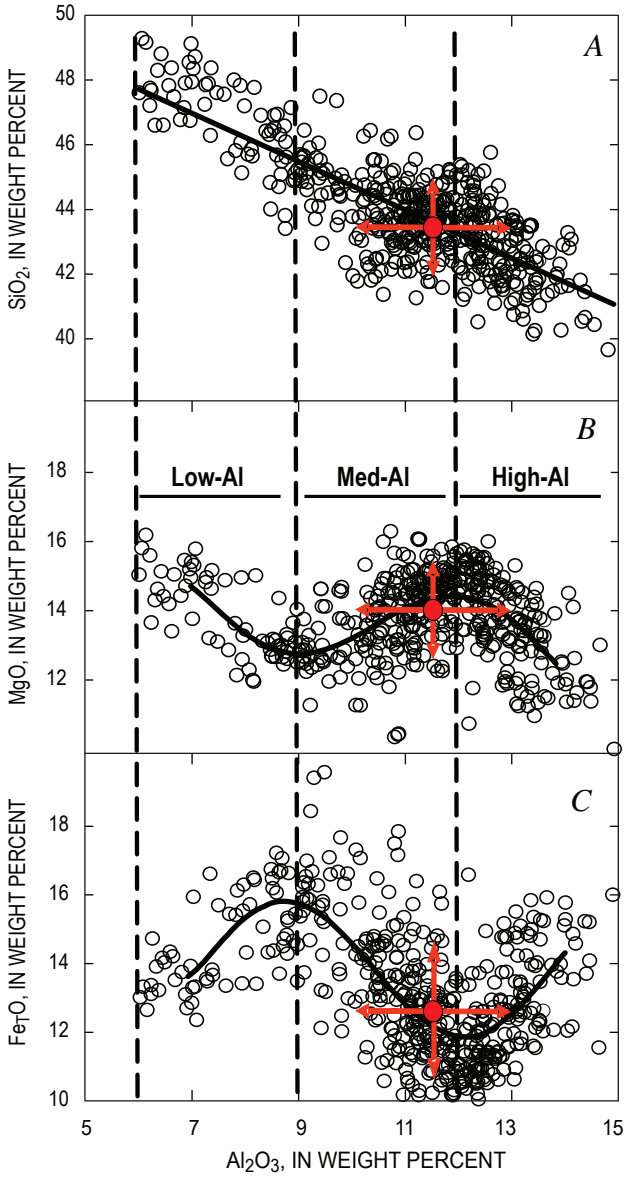

Figure 13. Alumina variation diagrams for Mount St. Helens 2004–6 amphibole phenocrysts (excluding data from crystals in lithic inclusions and glassy lithic fragments); average and 1σ standard deviation in red. Curves are high-order polynomial fits. *A*, Silica. *B*, Magnesia. *C*, Iron oxide (Fe_TO calculated as 100 percent ferrous iron). Reversals in Fe_TO and MgO with increasing Al_2O_3 define low-Al (6 to 9 percent), medium-Al (9 to 12 percent), and high-Al (>12 percent) compositions.

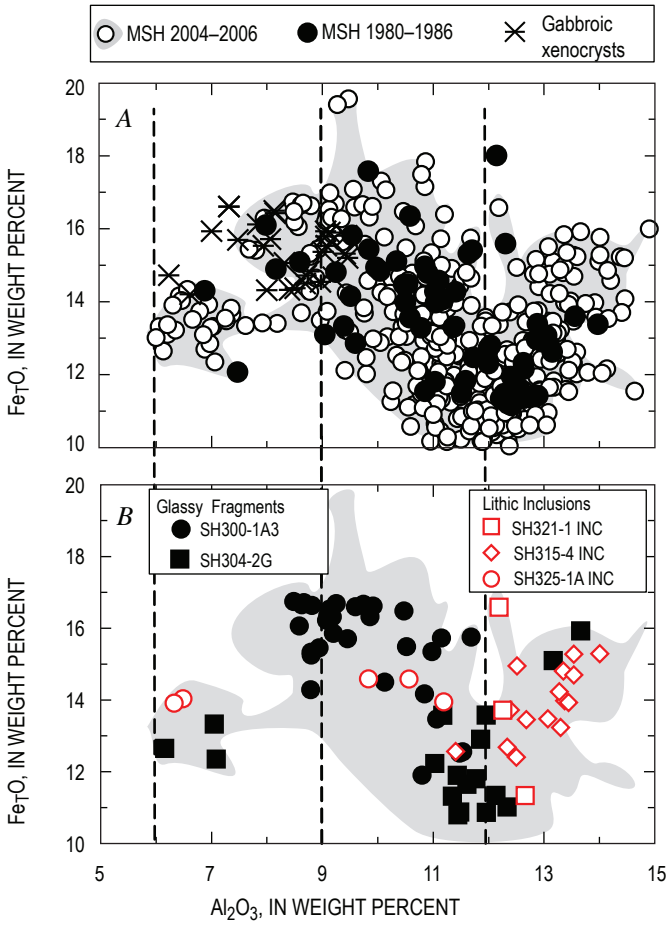

Figure 14. Iron oxide versus alumina in Mount St. Helens amphibole phenocrysts. *A*, 2004–6 amphibole phenocrysts (open circles and gray-shaded area) compared to those in 1980–86 Mount St. Helens dacite and gabbroic xenocrysts. *B*, Amphiboles in lithic inclusions and glassy lithic fragments; shaded area corresponds to field of 2004–6 amphibole phenocrysts shown in *A*.

Table 2. Selected electron microprobe analyses of amphibole phenocrysts in Mount St. Helens 2004–2006 dacite.

[Laboratories identified by first two letters in analysis number: AM, American Museum of Natural History; GS, U.S. Geological Survey, Denver; OS, Oregon State University. Relative position of analyzed spot: inZ, inner zone; outZ, outer zone. Nomenclature from Leake and others (1997): mghst, magnesiohastingsite; tscher, tschermakite; mghb, magnesiohornblende; eden, edenite; parg, pargasite. See appendix 2, table A2, for all analytical data.]

Sample No.--	SH304-2A			SH305-1			SH306-A		DRS_3_9_4		SH314-1		SH315-3			SH315-4		SH317-4	
Analysis No. ----------	OS-MR4-3	AM-G24C	AM-G24R	OS-MR3-2	OS-MR3-3	OS-MR3-4	OS-MR2-2	OS-MR2-5	GS-F3P13	GS-F3P9	GS-F3P1	GS-F3P5	GS-F16G1 P1	GS-F16G1 P2	GS-F16G1 P3	GS-F1G1 P1	GS-F1G1 P2	GS-F7G2 P2	GS-F1G2 P7
Position-------	core	core	rim	core	core	core	core	core	core	rim	core	rim	inZ	core	rim	core	rim	core	rim
SiO_2	48.4	42.0	44.0	43.1	42.9	46.9	42.6	47.8	43.1	47.9	42.6	47.1	43.7	44.0	45.1	42.2	43.3	40.5	42.3
TiO_2	1.54	2.53	2.39	2.37	2.24	2.09	1.97	1.46	2.21	1.46	2.37	1.48	1.46	1.61	0.88	2.38	2.11	3.06	2.35
Al_2O_3	7.4	12.8	12.5	14.2	14.0	8.6	13.1	7.9	12.2	6.9	12.4	6.9	9.4	8.5	8.0	12.1	11.2	14.4	13.2
FeO	13.7	11.3	10.7	14.6	12.0	13.7	14.8	13.4	10.8	12.7	10.9	13.1	16.3	16.2	16.3	10.4	9.9	13.7	13.1
MnO	0.3	0.1	0.1	0.12	0.13	0.16	0.20	0.28	0.12	0.23	0.12	0.24	0.35	0.29	0.35	0.11	0.11	0.17	0.12
MgO	15.2	14.7	15.5	11.6	14.5	14.4	12.0	15.0	14.8	14.7	14.9	15.5	12.4	12.7	13.3	15.3	16.1	11.9	13.3
CaO	11.0	11.2	11.4	10.4	10.3	11.3	11.2	10.6	10.8	10.8	11.5	11.2	10.4	10.4	9.8	11.1	11.1	11.3	10.7
Na_2O	1.5	2.4	2.4	2.4	2.6	1.8	2.1	1.7	2.5	1.5	2.8	1.8	1.8	2.1	1.6	2.9	2.8	2.6	2.6
K_2O	0.28	0.30	0.32	0.38	0.29	0.34	0.35	0.23	0.30	0.22	0.29	0.22	0.26	0.31	0.20	0.30	0.30	0.31	0.34
F	0.02	0.08	0.10	0.00	0.00	0.01	0.01	0.02	0.06	0.25	0.07	0.08	0.22	0.00	0.14	0.19	0.10	0.02	0.04
Cl	0.05	0.02	0.01	0.03	0.02	0.05	0.03	0.04	0.02	0.04	0.01	0.04	0.02	0.02	0.02	0.02	0.01	0.26	0.14
O = F,Cl	0.00	0.04	0.05	0.01	0.00	0.01	0.00	0.00	0.03	0.11	0.03	0.04	0.10	0.00	0.06	0.08	0.04	0.06	0.05
Total	99.19	97.37	99.38	99.19	99.11	99.33	98.36	98.39	96.94	96.63	97.99	97.60	96.20	96.16	95.56	96.98	97.03	98.28	98.25
T-Site Si^{+4}	6.869	6.074	6.209	6.176	6.088	6.690	6.189	6.830	6.242	6.969	6.149	6.862	6.490	6.587	6.717	6.144	6.271	5.929	6.119
T-Site $^{IV}Al^{+3}$	1.131	1.926	1.791	1.824	1.912	1.310	1.811	1.170	1.758	1.031	1.851	1.138	1.510	1.413	1.283	1.856	1.729	2.071	1.881
C-Site $^{VI}Al^{+3}$	0.105	0.250	0.284	0.576	0.437	0.141	0.432	0.165	0.331	0.153	0.258	0.041	0.128	0.089	0.114	0.213	0.186	0.412	0.376
C-Site Ti^{+4}	0.165	0.275	0.253	0.255	0.239	0.224	0.215	0.156	0.241	0.160	0.258	0.162	0.163	0.181	0.099	0.261	0.229	0.337	0.255
C-Site Fe^{+3}	0.620	0.772	0.660	0.643	0.704	0.585	0.673	0.667	0.642	0.571	0.591	0.370	0.963	0.621	0.896	0.626	0.615	0.536	0.681
C-Site Mg^{+2}	3.212	3.161	3.272	2.487	3.070	3.052	2.604	3.184	3.187	3.192	3.202	3.355	2.752	2.828	2.946	3.316	3.468	2.604	2.859
C-Site Fe^{+2}	0.901	0.527	0.522	1.036	0.546	0.999	1.077	0.826	0.599	0.925	0.691	1.072	0.995	1.281	0.946	0.584	0.502	1.108	0.827
B-Site Fe^{+2}	0.102	0.066	0.080	0.070	0.179	0.049	0.043	0.110	0.071	0.049	0.036	0.153	0.064	0.125	0.187	0.059	0.079	0.032	0.082
B-Site Mn^{+2}	0.033	0.011	0.010	0.015	0.015	0.019	0.025	0.034	0.014	0.028	0.015	0.029	0.044	0.037	0.044	0.013	0.014	0.022	0.015
B-Site Ca^{+2}	1.674	1.734	1.720	1.595	1.571	1.722	1.742	1.615	1.682	1.678	1.778	1.741	1.660	1.674	1.560	1.734	1.722	1.767	1.661
B-Site Na^{+}	0.192	0.189	0.191	0.319	0.235	0.209	0.190	0.242	0.233	0.245	0.171	0.076	0.232	0.164	0.209	0.195	0.185	0.179	0.243
A-Site Na^{+}	0.220	0.471	0.465	0.341	0.470	0.285	0.403	0.224	0.481	0.191	0.605	0.438	0.275	0.444	0.247	0.634	0.600	0.566	0.491
A-Site K^{+}	0.051	0.056	0.058	0.070	0.053	0.061	0.064	0.042	0.055	0.041	0.053	0.041	0.049	0.060	0.038	0.055	0.055	0.058	0.063
Total	15.27	15.53	15.52	15.41	15.52	15.35	15.47	15.27	15.54	15.23	15.66	15.48	15.32	15.50	15.28	15.69	15.65	15.62	15.55

Table 2. Selected electron microprobe analyses of amphibole phenocrysts in Mount St. Helens 2004–2006 dacite.—Continued

[Laboratories identified by first two letters in analysis number: AM, American Museum of Natural History; GS, U.S. Geological Survey, Denver; OS, Oregon State University. Relative position of analyzed spot: inZ, inner zone; outZ, outer zone. Nomenclature from Leake and others (1997): mghst, magnesiohastingsite; tscher, tschermakite; mghb, magnesiohornblende; eden, edenite; parg, pargasite. See appendix 2, table A2, for all analytical data.]

Sample No--	SH319-1			SH321-1			SH323-2		SH323-3				SH324-3				SH325-1		
Analysis No.----------	OS-MR2-1	OS-MR2-3	OS-MR3-1	GS-F0P3	GS-F2P3	OS-MR1-3	OS-MR2-3	OS-MR3-2	GS-G1-2	GS-G1-7	GS-G1-6	GS-G1-8	GS-F0P3	GS-F0P8	OS-MR1-1	OS-MR1-2	GS-F1B-G1P3	GS-F1B-G1P4	GS-F1B-G1P5
Position-------	core	core	core	core	core	core	core	core	core	inZ	outZ	rim	core	core	core	core	core	inZ	rim
SiO_2	44.3	45.2	43.4	43.7	43.5	44.8	46.4	42.8	43.6	43.7	44.2	43.8	42.7	45.6	44.5	43.5	44.9	42.0	44.9
TiO_2	2.24	2.13	2.38	2.48	2.74	2.55	1.31	2.79	2.19	2.20	2.17	2.78	2.42	1.11	2.51	2.27	1.63	2.31	1.71
Al_2O_3	11.7	12.3	13.2	10.8	9.8	10.3	9.2	14.2	10.9	12.3	11.7	10.1	11.6	9.4	11.0	13.4	9.0	12.7	9.1
FeO	12.3	10.6	11.7	11.1	13.7	13.7	17.0	13.5	13.6	11.6	10.5	12.9	14.8	15.6	13.1	12.7	13.5	12.7	13.7
MnO	0.17	0.12	0.10	0.14	0.15	0.19	0.27	0.13	0.19	0.15	0.12	0.19	0.20	0.26	0.16	0.12	0.21	0.15	0.23
MgO	14.6	15.6	14.5	15.0	13.8	13.9	12.5	12.6	13.2	14.5	15.2	13.7	12.3	13.5	13.8	13.9	14.0	13.0	13.8
CaO	11.2	10.9	11.1	11.1	10.7	11.0	11.0	10.9	10.8	10.8	10.9	10.5	10.8	10.0	11.4	11.1	10.8	10.8	10.6
Na_2O	2.2	2.3	2.4	2.3	2.7	2.0	1.9	2.4	2.3	2.3	2.3	2.3	2.6	1.9	2.1	2.4	2.4	2.4	1.9
K_2O	0.29	0.29	0.32	0.25	0.29	0.31	0.24	0.36	0.25	0.30	0.28	0.30	0.29	0.23	0.31	0.34	0.24	0.28	0.23
F	0.00	0.00	0.00	0.02	0.03	0.00	0.00	0.01	0.69	0.16	0.10	0.19	0.02	0.04	0.01	0.00	0.04	0.01	0.03
Cl	0.02	0.01	0.02	0.18	1.55	0.04	0.02	0.02	0.02	0.01	0.01	0.02	0.11	0.16	0.02	0.02	0.17	0.11	0.19
O=F,Cl	0.00	0.00	0.00	0.05	0.35	0.01	0.00	0.00	0.29	0.07	0.04	0.08	0.03	0.05	0.00	0.00	0.05	0.03	0.06
Total	98.88	99.53	99.16	97.17	98.59	98.72	99.83	99.71	97.34	98.08	97.31	96.61	97.85	97.82	98.91	99.64	96.81	96.39	96.32
T-Site Si^{+4}	6.312	6.343	6.165	6.341	6.395	6.430	6.665	6.097	6.388	6.261	6.360	6.431	6.270	6.609	6.381	6.167	6.593	6.181	6.599
T-Site $^{IV}Al^{+3}$	1.688	1.657	1.835	1.659	1.605	1.570	1.335	1.903	1.612	1.739	1.640	1.569	1.730	1.391	1.619	1.833	1.407	1.819	1.401
C-Site $^{VI}Al^{+3}$	0.268	0.369	0.369	0.192	0.087	0.172	0.213	0.473	0.267	0.346	0.334	0.172	0.277	0.210	0.240	0.408	0.147	0.379	0.177
C-Site Ti^{+4}	0.240	0.225	0.254	0.270	0.303	0.276	0.142	0.298	0.242	0.238	0.234	0.307	0.267	0.120	0.271	0.242	0.180	0.256	0.189
C-Site Fe^{+3}	0.700	0.615	0.671	0.613	0.492	0.665	0.687	0.623	0.620	0.685	0.620	0.610	0.585	0.884	0.573	0.681	0.629	0.622	0.716
C-Site Mg^{+2}	3.092	3.273	3.074	3.233	3.017	2.968	2.666	2.681	2.877	3.108	3.251	2.990	2.682	2.917	2.958	2.929	3.073	2.857	3.016
C-Site Fe^{+2}	0.697	0.514	0.631	0.673	1.100	0.916	1.292	0.926	0.995	0.623	0.560	0.921	1.190	0.864	0.959	0.742	0.972	0.886	0.902
B-Site Fe^{+2}	0.063	0.117	0.081	0.060	0.091	0.068	0.060	0.064	0.055	0.083	0.077	0.052	0.043	0.148	0.045	0.082	0.056	0.061	0.072
B-Site Mn^{+2}	0.021	0.014	0.012	0.017	0.019	0.024	0.033	0.016	0.024	0.018	0.015	0.023	0.025	0.032	0.020	0.014	0.025	0.018	0.029
B-Site Ca^{+2}	1.709	1.645	1.689	1.724	1.692	1.686	1.691	1.667	1.690	1.665	1.676	1.657	1.700	1.559	1.746	1.679	1.695	1.706	1.673
B-Site Na^{+}	0.207	0.224	0.218	0.200	0.198	0.222	0.217	0.253	0.231	0.234	0.232	0.267	0.232	0.260	0.190	0.224	0.224	0.215	0.226
A-Site Na^{+}	0.391	0.391	0.446	0.449	0.563	0.343	0.324	0.399	0.425	0.413	0.399	0.384	0.513	0.270	0.399	0.424	0.450	0.469	0.315
A-Site K^{+}	0.053	0.053	0.059	0.047	0.054	0.057	0.045	0.066	0.047	0.054	0.051	0.056	0.053	0.042	0.056	0.062	0.045	0.052	0.043
Total	15.44	15.44	15.50	15.50	15.62	15.40	15.37	15.46	15.47	15.47	15.45	15.44	15.57	15.31	15.46	15.49	15.50	15.52	15.36
Name	tscher	tscher	mghst	tscher	mghst	tscher	mghb	tscher	tscher	tscher	tscher	tscher	mghst	mghb	tscher	tscher	mghb	mghst	mghb

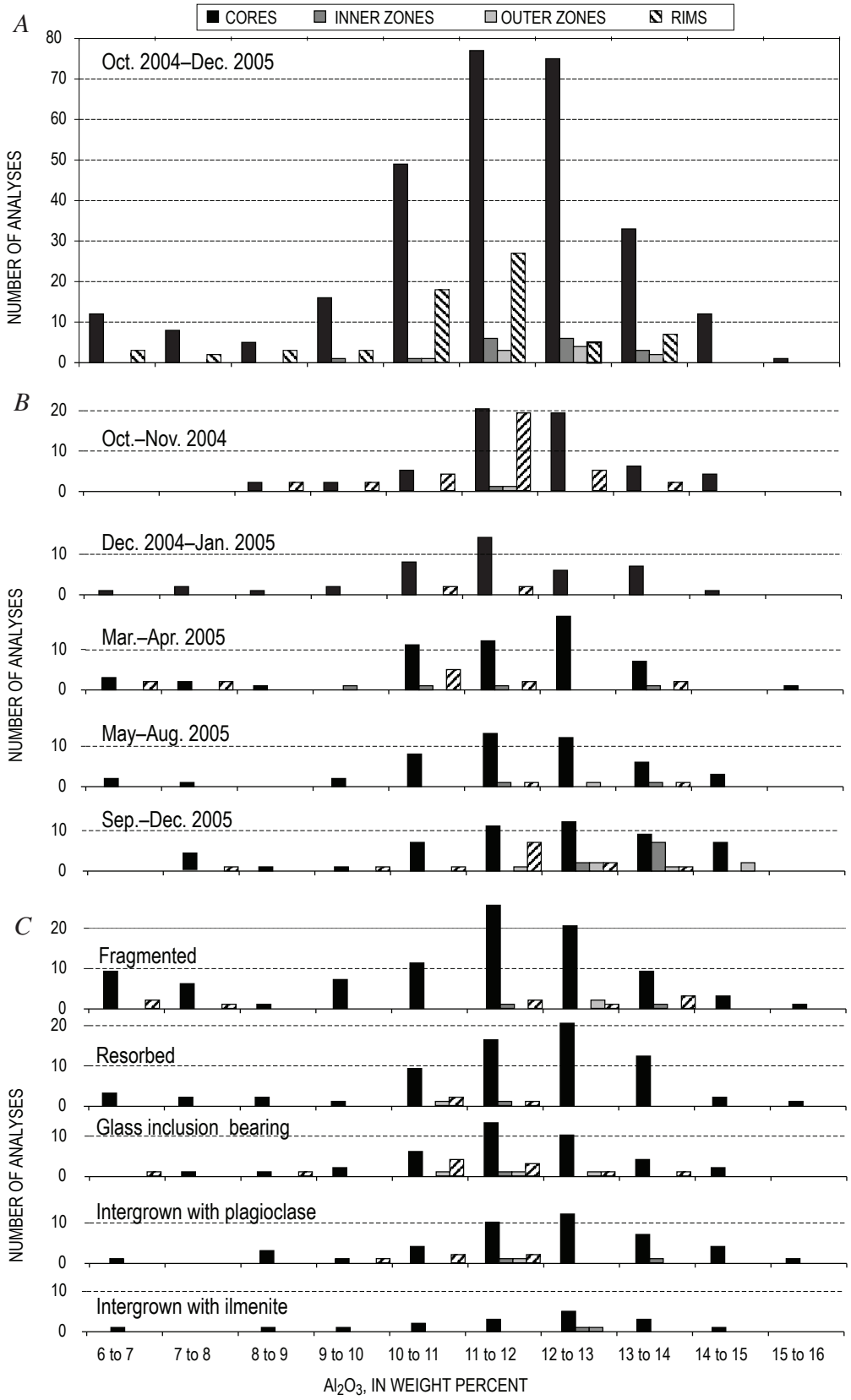

Figure 15. Histograms showing the frequency distribution of Al_2O_3 in cores, inner zones, outer zones, and rims of amphibole crystals in Mount St. Helens 2004–6 dacite lava (excluding crystals in glassy lithic fragments and lithic inclusions). *A,* For all 2004–6 amphiboles. *B,* For consecutive time intervals. *C,* For phenocrysts with specific textural attributes.

crystallized from andesite at high pressures (for example, Allen and Boettcher, 1978; Grove and others 2003). High-Al amphibole compositions, along with differences in reaction textures, are consistent with these inclusions originating from an andesite magma (Pallister and others, this volume, chap. 30), but there is no clear evidence in support of a comagmatic relation between the andesitic magma and the host dacite.

The one dacitic inclusion studied (SH321-1inc) has a range of amphibole chemistry similar to that of 1980–86 and 2004–6 lava. As inferred from the presence of clinopyroxene and the distinctly thick amphibole reaction rims (see reaction-rim discussion), this inclusion could be an accidental piece of shallow 1980s conduit material.

The frequency distribution of alumina concentrations in cores, inner zones, outer zones, and rims of amphiboles in the 2004–6 dacite indicate an approximately normal distribution about the mean value of 11.4±1.7 percent Al_2O_3 (fig. 15). A similar distribution is observed for a smaller population of 1980–86 amphiboles, but amphiboles in gabbroic xenoliths overlap the low end of the 2004–6 population (fig. 14*A*).

Correlations between alumina content and size of amphibole crystals reveal a normal distribution about the mean alumina content of ~11 percent and about a median size range within 10–100×10^3 μm^2 (fig. 2), suggestive of compositional and morphologic consistency of the mean population. In contrast, most of the crystal fragment population (gray bars in fig. 2) has low-Al compositions, supporting the likelihood of a xenocrystic origin. There is no clear correlation between alumina content and acicularity. Both equant and relatively acicular populations have nearly similar distributions about the alumina average.

The abundance of low- to high-Al amphiboles, just as the overall amphibole modal abundance and bulk-dacite composition, has not changed throughout the duration of the 2004–6 eruption (fig. 15). Furthermore, the same overall distribution of alumina contents is apparent among amphiboles of similar texture or mineral associations (fig. 15).

Multiple analyses from core to rim were obtained for numerous amphibole crystals. The compositional variation of amphibole rims within and among samples is similar to the broad range of core compositions and the amphibole population as a whole (fig. 16). Detailed analyses of amphiboles with multiple growth zones reveal some systematic tendencies within limited populations of crystals. For example, analyses of cores, inner zones, and outer zones of several SH323-3 amphiboles vary widely and are without obvious correlations of core-to-rim progressions between crystals, but the rims all trend toward an average 10.8±0.6 percent Al_2O_3 (fig. 16*A*). This convergence of rims toward the amphibole composition to last equilibrate with the host magma is within the 1σ uncertainty of the 11.4 percent average of Al_2O_3 in all 2004–6 amphiboles. Such is not the case for core-to-rim analyses of crystals in SH325-1A (fig. 16*B*), which are similar to the overall broad dispersion of rim data. The variable rim compositions must reflect changing conditions in the magma reservoir and during ascent from it.

Amphibole Rare-Earth-Element (REE) Chemistry

The REE concentrations in all 2004–6 dacite amphibole phenocrysts display middle rare-earth-element (MREE) enrichment patterns typical of igneous clinoamphiboles (fig. 17; appendix 2). Similar MREE-enriched patterns for different crystals in each sample are distinguished by varying degrees of overall REE enrichment, accompanied by progressive Eu depletion. Like other amphibole characteristics discussed above, there are no clear distinctions of REE patterns among samples over time or, in most cases, with textural attributes. However, a distinct trend of overall REE enrichment (typified by La) and Eu depletion (relative to Nd) with decreasing alumina content in medium- to low-Al amphibole crystals is clearly observed (fig. 18).

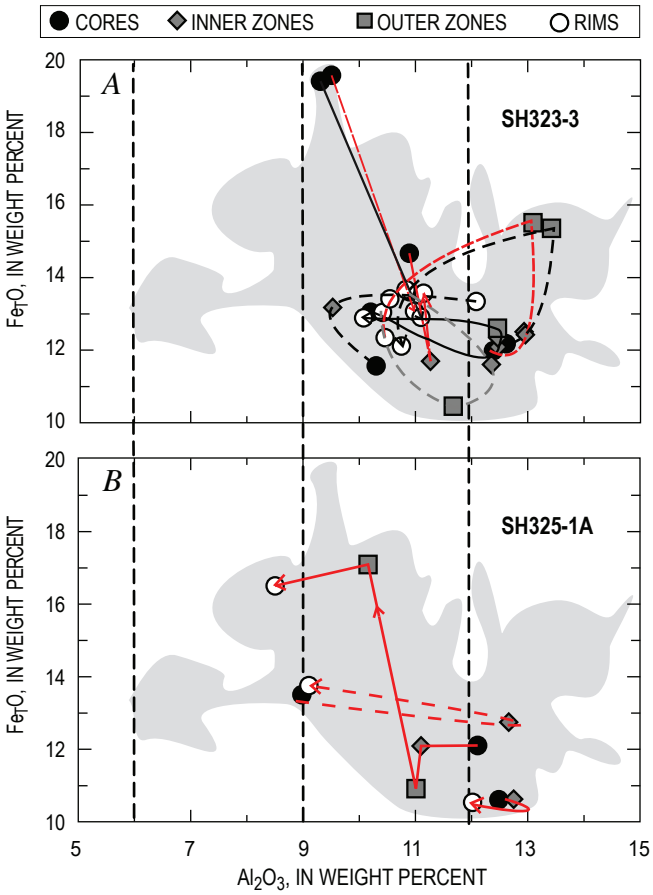

Figure 16. Iron oxide (Fe_TO) versus alumina within individual amphibole phenocrysts in Mount St. Helens 2004–6 dacite lava. Arrows connect core, inner-zone, outer-zone, and rim compositions. Shaded area is the field of 2004–6 amphibole phenocrysts from figure 14*A*. *A*, Interior compositions of amphiboles vary widely, but rim compositions converge toward an average of 10.8±0.6 percent Al_2O_3. *B*, Example of amphiboles that do not show consistent variations.

Concentration patterns for the REE-enriched and Eu-depleted (Eu/Nd<1) amphibole crystals suggest that some are not comagmatic (fig. 19). The three most extreme patterns (from samples SH304-2A, SH305-1, SH311-1B) are all low-Al amphiboles (7.4–8.9 percent Al_2O_3) with patchy zoning and variable resorption (for example, fig. 4*A*). They must be derived from a strongly Eu-depleted melt that has undergone significant Eu^{3+}-enriched plagioclase crystallization in an oxidizing environment. Such distinctive REE patterns suggest that these low-Al amphiboles are xenocrysts. New trace-element data for gabbroic xenoliths, in which amphibole is a late cumulus phase, would help to test this hypothesis.

There are no textural distinctions among the group of slightly LREE-enriched, low- to medium-Al amphiboles with Eu/Nd <1 (fig. 18*B*). The slight REE enrichment reflects a normal magmatic fractionation trend from one or more dacite magmas. Low-Al amphiboles with slight Eu depletion may have been derived from earlier generations of solidified dacite accumulated at the top of the Mount St. Helens magma reservoir or by shallow low-temperature crystallization within the host magma. For the medium- to high-Al amphiboles, the most prevalent of our 2004–6 samples, LREE concentrations are consistently low, and Eu is not depleted relative to Nd.

Amphibole Stoichiometry and Nomenclature

The amphibole nomenclature used here, as recommended by the International Mineralogical Association, is that of Leake and others (1997). Nomenclatorial guidelines are based upon occupancies of the A, B, C, and T sites within the amphibole mineral structural formula,

$$\mathbf{A}[\mathrm{Na+K})\ \mathbf{B}\mathrm{Ca}_{2-x}\ [x=\mathrm{Mg, Fe^{2+}, Mn, Mg})\ \mathbf{C}^{\mathbf{M1,M2,M3}}\ \mathrm{Mg}_{5-y}\ [y=\mathrm{Fe^{2+}, Mn, {}^{VI}Al, Ti, Fe^{3+}}]\ \mathbf{T}\mathrm{Si}_{8-z}\ [z={}^{\mathrm{IV}}\mathrm{Al}]\ \mathrm{O}_{22}\ \mathrm{OH}_{2-n}\ [n=\mathrm{F, Cl}]).$$

Herein, the Leake and others (1997) nomenclature was applied to the amphibole stoichiometry determined using the Holland and Blundy (1994) method. This method was chosen because it allows for each amphibole to be normalized to the best stoichiometric constraint for ferric iron determination and gives the most reasonable amphibole formula for calculating pressure using the Anderson and Smith (1995) Al-in-hornblende barometer. Leake and others (1997) propose a method for calculating amphibole formula from electron microprobe analysis that is similar to that of Holland and Blundy (1994). Amphibole classification using the two methods typically results in the same name except for species that are sensitive to ferric iron determinations, such as pargasite and magnesiohastingsite.

The complete 2004–6 amphibole data set, plotted using the classification diagram of Leake and others (1997), is shown in figure 20. High-silica, low-Al amphiboles in dacite and gabbroic xenoliths are magnesiohornblende, but they also include some alkaline, edenite compositions. Medium- to high-Al ranges of the data set fall in tschermakite to magnesiohastingsite fields. The medium-Al group, consisting mostly of tschermakite, gives way to magnesiohastingsite with increasing alumina and alkali contents, extending toward rare pargasite compositions. Aside from mineral classification, the main purpose of calculating amphibole stoichiometry is to evaluate crystallographically controlled cationic variations that are sensitive to pressure and temperature.

As is widely documented in studies of clinoamphibole thermobarometry of igneous and metamorphic rocks, the extent of Tschermak's molecule substitution is a function of relative pressure and temperature of equilibration (Helz, 1982; Hammarstrom and Zen, 1986; Anderson and Smith, 1995; Bachmann and Dungan, 2002). At higher pressures and temperatures, the amount of Al in octahedral (C) sites (^{VI}Al) increases together with the amount in tetrahedral Al (^{IV}Al) sites. Most of this coupled alumina substitution occurs at the expense of divalent cations (for example, Mg^{2+} and Fe^{2+}) in the octahedral C-site and silica in tetrahedral sites in a pressure-sensitive Al-Tschermak exchange (^{C}(Mg,Fe) + ^{T}Si ↔ ^{IV}Al+^{VI}Al). At higher temperatures, increased concentrations of alkali cations (Na^+ and K^+) and Ti^{4+} are accommodated with additional ^{IV}Al in the amphibole lattice and form edenite (^{A}vacancy + ^{T}Si ↔ ^{A}(Na+K) + ^{IV}Al) and Ti-Tschermak (^{B}Mn+2^{T}Si ↔ ^{C}Ti+2^{IV}Al) substitutions. There is a broad, continuous range of pressure-sensitive Al-Tschermak component substitution exhibited by the complete array of amphibole compositions in 2004–6 Mount St. Helens dacite (fig. 21*A*). In addition, a broad range of temperature-sensitive Ti-Tschermak and edenite cationic exchanges also are apparent (figs. 21*B–D*).

The amphibole calculation optimizes ferric iron (Fe^{3+}) in the stoichiometric scheme and is a means of "ironing out" the secondary deviations in total iron and magnesium with alumina (figs. 13*B*, 13*C*). The exchange of Fe^{2+} and Mg^{2+} in the C site is consistently linear in high- and medium-Al amphiboles (fig. 22). At higher alumina contents and consistent with Al-Tschermak substitution, the absolute concentrations of Mg and Fe^{2+} are lower along lines of constant Mg number (Mg#, 100*(Mg/(Mg+ Fe^{2+})). The Mg# variation in low-Al amphibole is more erratic. The Mg# increases with increasing proportion of Fe^{3+} (fig. 23*A*), suggesting that the Mg# trends are at least partly affected by differences in the oxidation state of host magmas. The variations of Ti and Mn with Mg# reveal distinctly different trends of low-Al magnesiohornblendes and the prevalent medium- to high-Al tschermakites and magnesiohastingsites (figs. 23*B*, 23*C*). Inverse trends of Ti versus Mg# (or Fe^{3+}) exhibited by the range of common amphibole compositions (±1σ population trend in fig. 23) are consistent with growth at variable temperature and f_{O_2} under buffered conditions, as suggested by temperature-f_{O_2} ranges calculated for Fe-Ti oxide pairs in 2004–6 dacite (Pallister and others, this volume, chap. 30, fig. 13).

Within the dataset there is no clear correlation between the Mg# and the relative partitioning of ^{VI}Al and ^{IV}Al (Al-

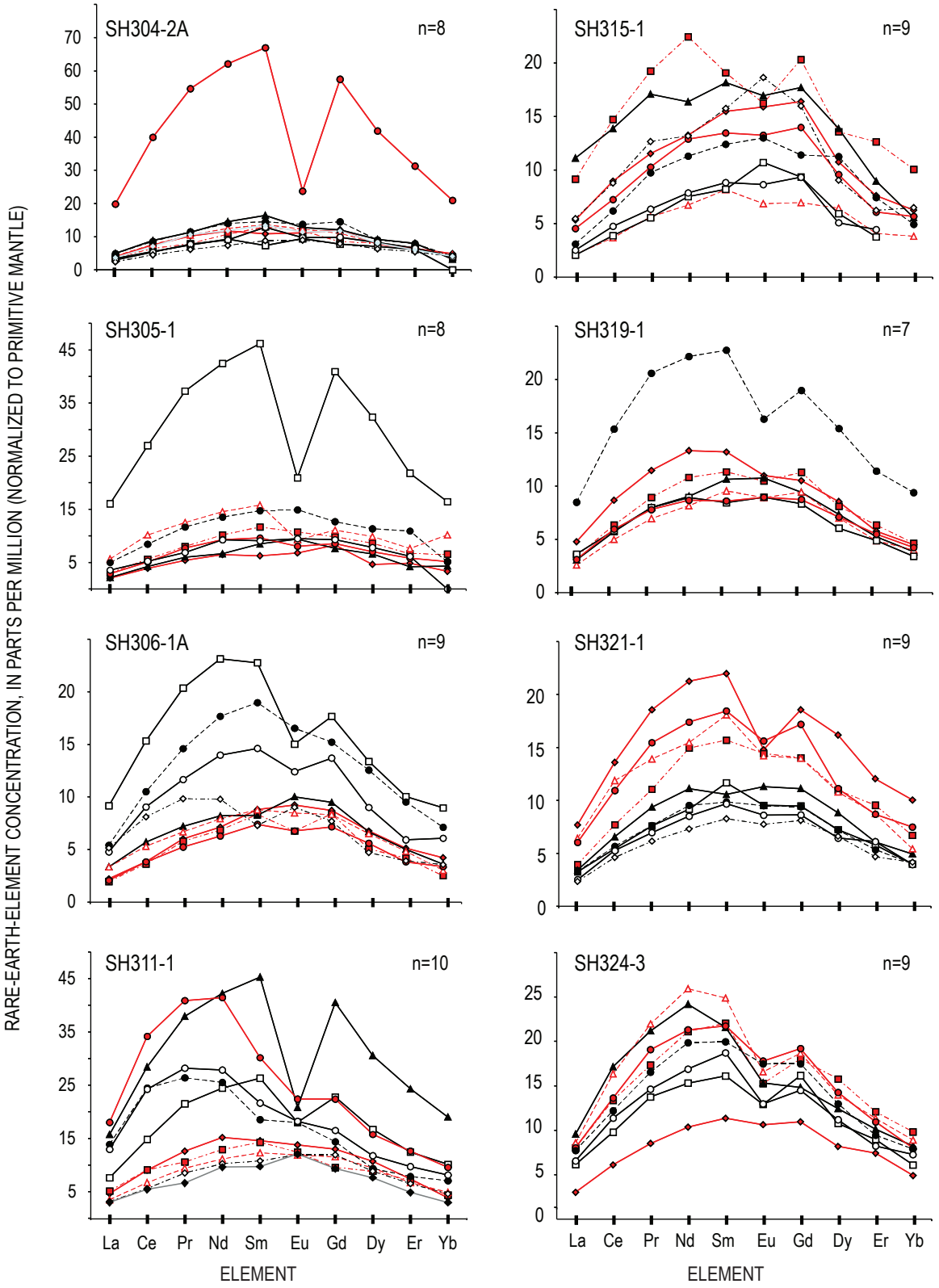

Figure 17. Rare-earth-element (REE) concentrations of amphibole phenocryst cores in eight consecutive Mount St. Helens 2004–6 dacite lava samples (normalized to "primitive mantle" of Sun and McDonough, 1989). Spidergrams show middle REE enrichment patterns that are typical of clinoamphibole and distinguished by varying degrees of REE enrichment and Eu depletion. Number of analyzed grains indicated (for example, n=8).

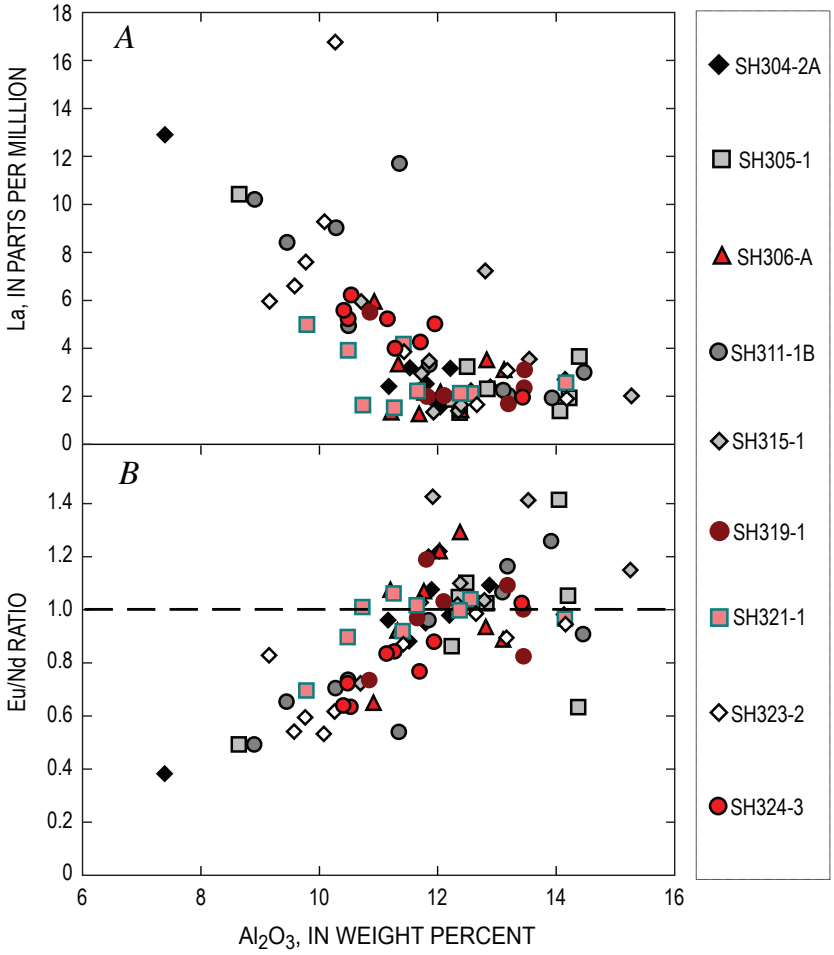

Figure 18. Rare-earth element (REE) versus alumina among amphibole phenocryst cores in consecutive Mount St. Helens 2004–6 dacite lava samples, showing trends reflective of overall REE enrichment and Eu depletion with decreasing alumina in medium- to low-Al amphiboles. *A*, La versus alumina. *B*, Eu/Nd versus alumina; Eu/Nd values <1 are Eu depleted.

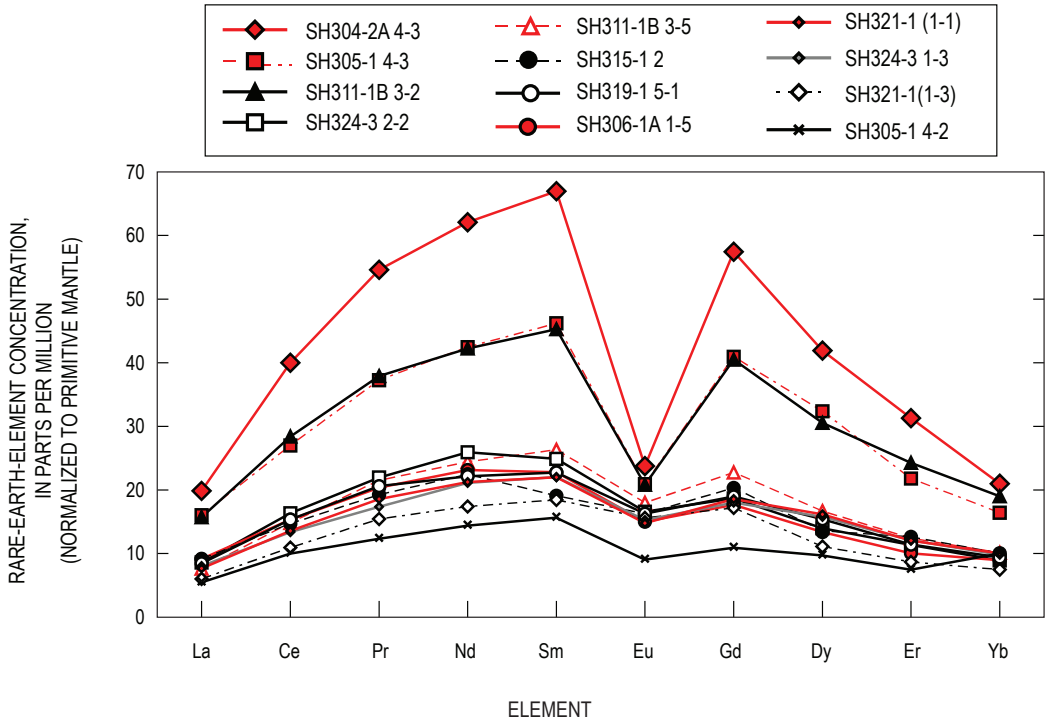

Figure 19. Rare-earth-element (REE) concentrations in Eu-depleted 2004–6 amphibole phenocrysts (normalized to "primitive mantle" of Sun and McDonough, 1989). Samples with the three most extreme REE patterns, likely xenocrysts, have low Al (7.4–8.9 percent Al_2O_3), patchy zoning, and resorbed edges.

Tschermak exchange; fig. 23*D*), indicating that Mg-Fe exchange is independent of relative pressure of crystallization. Also, no consistent differences are observed between core and rim Mg# and ^{VI}Al or ^{IV}Al. These observations and interpretations are in contrast to the inverse relation of Mg# and ^{IV}Al documented within individual 2004–6 amphibole crystals by Rutherford and Devine (this volume, chap. 31). The covariance of Mn, Ti, and Fe^{2+} in the medium- to high-Al amphibole suite likely reflects differences in the abundance and composition of coexisting Fe-Ti oxides in the crystallizing assemblage, which are affected by changes in temperature and the oxidation state over a range of pressures reflected by Al-Tschermak substitution.

Amphibole Thermobarometry

Rutherford and Devine (this volume, chap. 31) conducted phase-equilibria experiments on 2004 dacite that establish lower P_{H_2O} and upper *T* limits of amphibole+plagioclase+orthopyroxene+Fe-Ti-oxide saturation. Their results reproduce the observed phenocrysts of the dacite between pressures of 130 and 300 MPa (~5–12 km depth) at 850°C to 920°C, respectively (Rutherford and Devine, this volume, chap. 31, fig. 10). They observed increased Tschermak component of Mount St. Helens amphibole equilibrated at 200–300 MPa and 900°C in comparison with that at or below 200 MPa at ~860–850°C. These data suggest that the Tschermak and edenite substitutions, exhibited by the predominant 2004–6 tschermakite and magnesiohastingsite compositions, ought to constrain the relative *P–T* path of dacite magmas that have contributed to the phenocryst mix observed in new lava.

The Al-in-hornblende thermobarometer of Anderson and Smith (1995) is used here to estimate relative equilibration pressures over the ~850–900°C temperature range established by iron-titanium oxide thermometry and experimental petrology of new dacite lava (Pallister and others, this volume, chap. 30; Rutherford and Devine, this volume, chap. 31). As expressed by Anderson and Smith (1995, p. 554) and debated by others (for example, Blundy and Holland, 1990; Rutherford and Johnson, 1992; Hammarstrom and Zen, 1992), this algorithm may not yield accurate results at temperatures in excess of experimental calibration (800°C) and without all of the Tschermak-buffering phases in the barometric assemblage. We assume that most amphiboles in the 2004–6 dacite were crystallized from similar dacite magmas at temperature <920°C and that all were cosaturated with fluid, plagioclase, orthopyroxene, and oxide. The covariance of alumina and silica in these phases is not fixed for every amphibole that crystallizes, but the Tschermak molecular substitution should be constrained by this same five-phase assemblage throughout the pressure range in which the amphibole crystallized, thus providing a relative indication of crystallization pressures and temperatures.

Calculated pressures for amphiboles equilibrated under known *P* and *T* conditions help validate application of Al-in-hornblende thermobarometry to Mount St. Helens dacite (fig. 24). The Anderson and Smith (1995) algorithm is accurate for the 200- to 800-MPa range of experimental amphiboles at

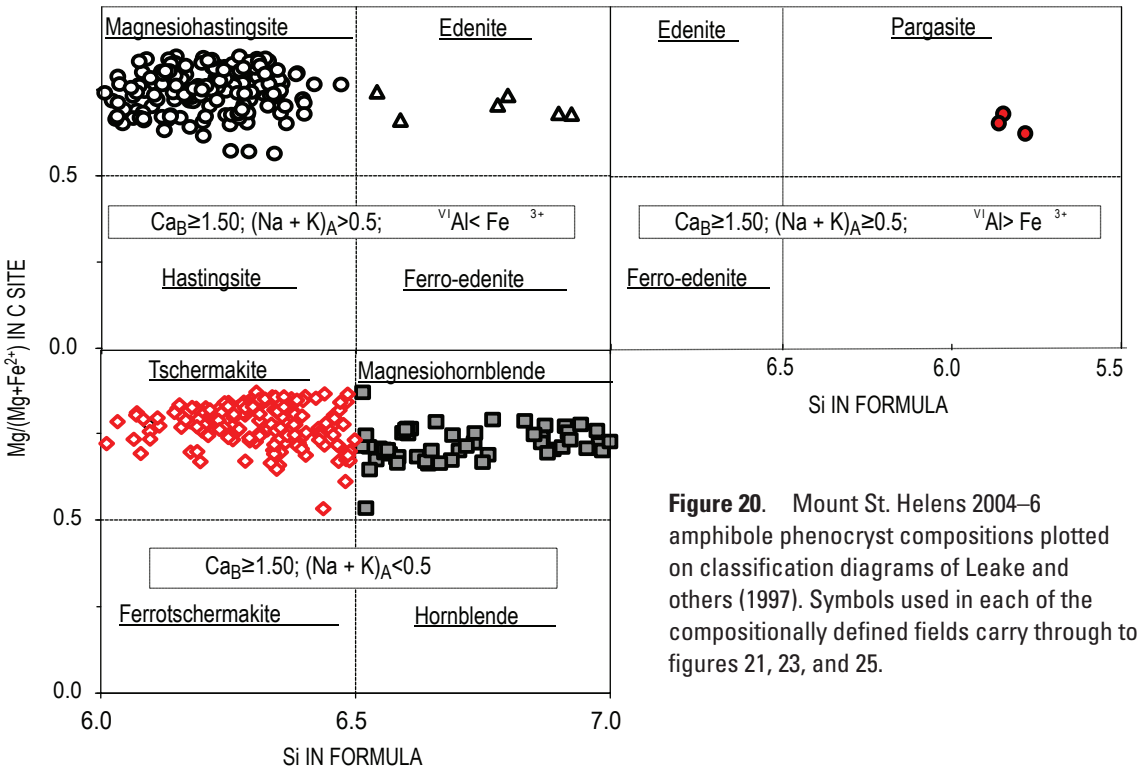

Figure 20. Mount St. Helens 2004–6 amphibole phenocryst compositions plotted on classification diagrams of Leake and others (1997). Symbols used in each of the compositionally defined fields carry through to figures 21, 23, and 25.

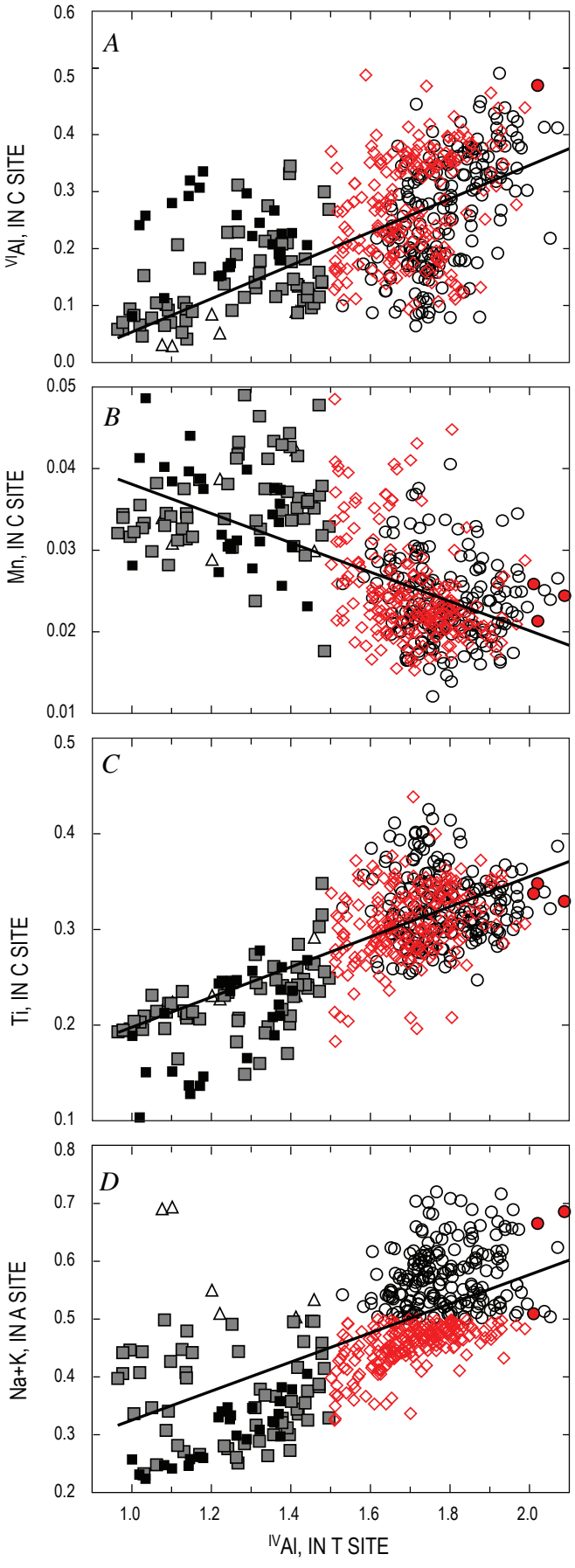

Figure 21. Site-specific cation concentrations versus tetrahedrally coordinated Al (^{IV}Al) in Mount St. Helens 2004–6 amphibole phenocrysts grouped according to amphibole type, with symbols as defined in figure 20. Magnesiohornblendes of 1986 gabbroic xenoliths, shown with black squares, are included for comparison. Lines shown represent best-fit linear regressions. *A*, Increasing octahedral alumina (^{VI}Al) concentrations roughly coincide with increasing tetrahedral alumina (^{IV}Al), reflecting a range of pressure-sensitive Al-Tschermak substitution. *B* and *C*, Antithetic variations of Mn and Ti with increasing ^{IV}Al demonstrate a continuous range of temperature-sensitive Ti-Tschermak substitution. *D*, Total alkali concentrations (Na+K in A site) increase with increasing ^{IV}Al in an edenite exchange, also indicative of increasing temperature of crystallization.

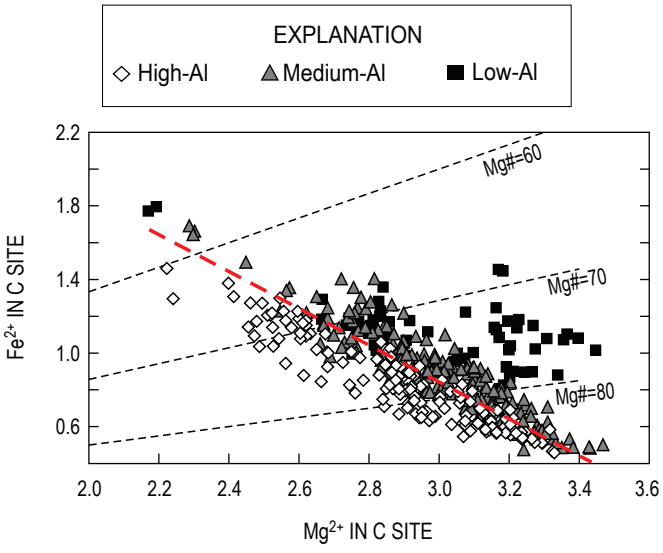

Figure 22. Fe^{2+} versus Mg^{2+} variation diagram for low-Al, medium-Al, and high-Al groups of Mount St. Helens 2004–6 amphiboles. At higher alumina contents, concentrations of Mg and Fe^{2+} (in C sites) are lower along lines of constant Mg# (=Mg/(Mg+Fe^{2+}), shown as dashed black lines. A well-balanced Fe-Mg C-site exchange is observed among medium-Al to high-Al amphiboles. The dashed red line shows best-fit linear regression of predominant 2004–6 amphibole population (defined as ±1σ from average composition).

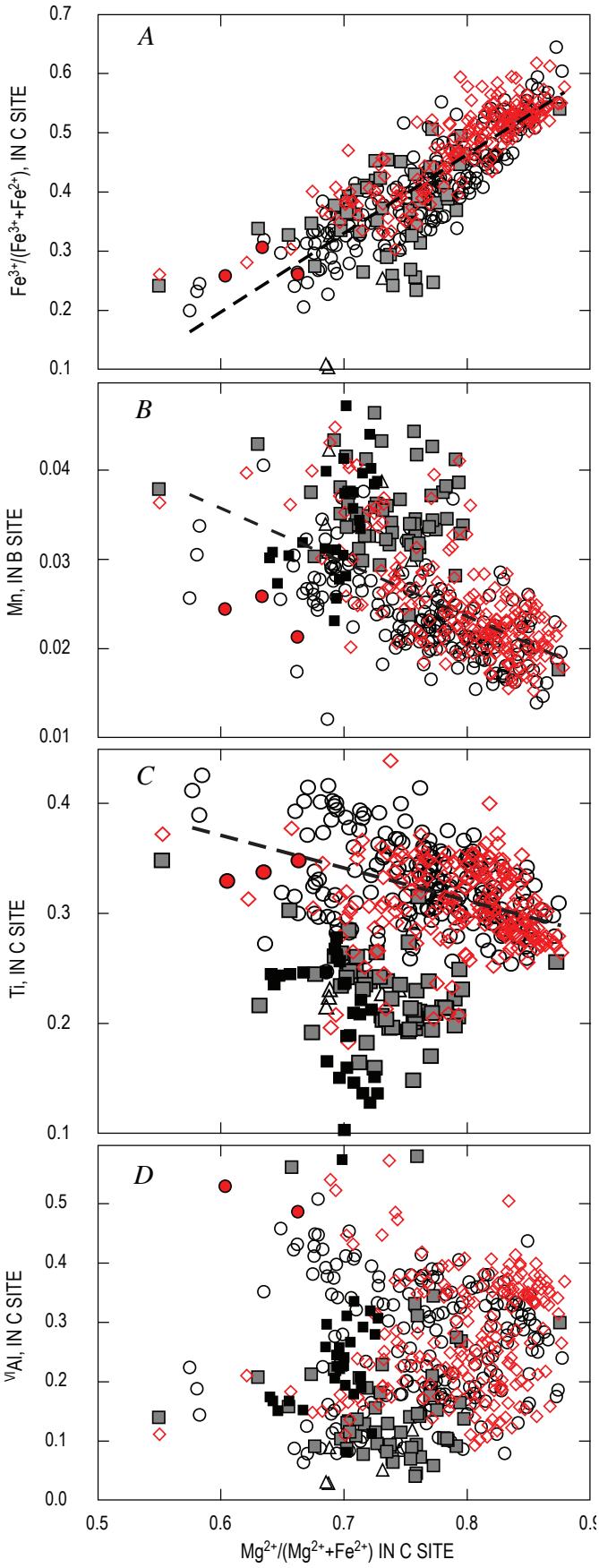

Figure 23. Site-specific cation concentrations versus Mg# in C site ($Mg^{2+}/(Mg^{2+}+Fe^{2+})$) in Mount St. Helens 2004–6 amphibole phenocrysts, grouped according to amphibole type, with symbols as defined in figure 20. Dashed lines represent best-fit linear regressions of predominant 2004–6 amphibole population (defined as ±1σ from average). Magnesiohornblendes in 1986 gabbroic xenoliths, shown as black squares, are presented for comparison. *A*, Mg# increases with increasing proportion of Fe^{3+} relative to total iron (Fe^{3+} + Fe^{2+}), suggesting that Mg# is largely affected by magmatic oxidation state. *B* and *C*, Covariance of Mn and Ti with Mg# in predominant amphibole population indicates Mg# varies independently of temperature-sensitive Ti-Tschermak exchange (figs. 21*B*, 21*C*). *D*, Octahedral alumina (^{VI}Al) concentrations show no systematic correlation with Mg#, indicating that Fe^{2+}-Mg exchange is independent of pressure-sensitive Al-Tschermak substitution.

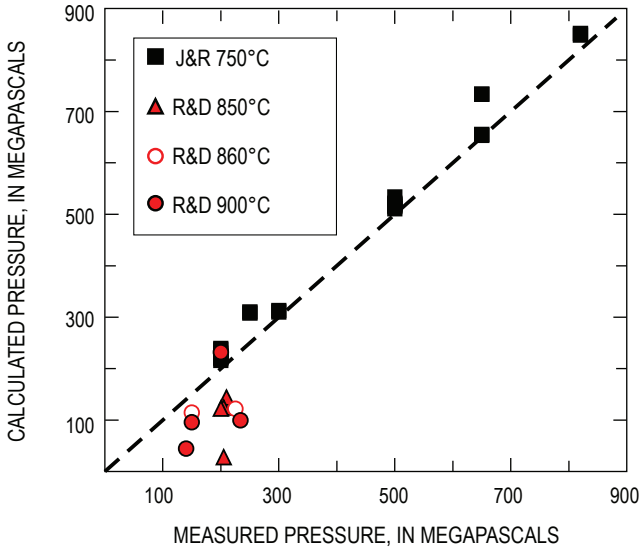

Figure 24. Plot of experimentally measured pressures versus pressures calculated by Al-in-hornblende barometer of Anderson and Smith (1995), using temperatures and amphibole compositions from experimental runs. J&R, Johnson and Rutherford (1989) experiments at 750°C on dacite from Fish Canyon Tuff (64.4 percent SiO_2) and Round Valley, Idaho (65.2 percent SiO_2), in which amphibole coexists with melt, fluid, quartz, biotite, plagioclase, sphene, and Fe-Ti oxides. R&D, Rutherford and Devine (this volume, chap. 31) experiments on 2004 Mount St. Helens dacite at 850°C, 860°C, and 900°C in which amphibole coexists with melt, fluid, plagioclase, orthopyroxene and Fe-Ti oxides.

740°C in three calc-alkaline magma compositions (64.4–65.2 percent SiO_2, Johnson and Rutherford, 1989) for which it was calibrated. In those experiments, the coexisting phase assemblage (melt, fluid, quartz, biotite, plagioclase, alkali-feldspar, sphene, and Fe-Ti oxides) provides a complete Tschermak-buffering capacity (Anderson and Smith, 1995). In experiments on 2004 Mount St. Helens dacite at pressures of 100–200 MPa and temperatures of 850–860°C and 900°C (Rutherford and Devine, this volume, chap. 31), amphibole coexists with a fluid+melt+plagiclase+orthopyroxene+oxide assemblage, similar to that of newly erupted lava. Overall, barometric calculations for amphibole equilibrated in the silica undersaturated dacite (analyses from table 6 of Rutherford and Devine, this volume, chap. 31) yield results consistent with the <200 MPa run conditions. Most of the estimates are low by more than 50 MPa, but there is closer agreement for the highest-Al amphiboles in runs at both 900°C and 850°C.

Barometric calculations for the predominant 2004–6 amphibole population (±1σ range, fig. 25) define a depth range for crystallization from 13.5 to ~4 km depth (350 MPa to 100 MPa) at temperatures between 850°C and 900°C. The overall average of phenocryst compositions yields barometry results of 220 MPa at 850°C. As restricted by the minimum pressure of amphibole stability (100 MPa), our calculations show that the bulk of amphibole crystallization occurred at temperatures less than ~875°C. At ~900°C, only high-Al amphiboles yield tenable calculated pressures, ranging from 100 to ~250 MPa, and perhaps to 300 MPa. Judging from the apparent error in applying Al-barometry to experimentally produced amphiboles at <200 MPa (fig. 24), it may be that actual equilibration pressures are higher by about 50–100 MPa. At 850°C this correction would increase the maximum depth range of average amphibole crystallization from ~8.5 km (220 MPa) to ~10.5 or perhaps to 12.5 km (270–320 MPa) and would increase the maximum depth range of the more aluminous tschermakite and magnesiohastingsite to >15 km (400 MPa).

The relative calculated pressures for the majority of amphibole compositions suggests two *P-T* scenarios for the 2004–6 magma and for prior generations of hostlike, precursory magma that are preserved in the crystal-laden mixture: (1) high-Al amphiboles formed at relatively low temperature and great depth (>15 km at <850°C), and the subsequent bulk of amphibole crystallization occurred during nearly isothermal ascent, or (2) crystallization during cooling between 900°C and 800°C at shallower depths within the magma reservoir (from 4 km to ~8 or possibly ~10 km), or a combination of (1) and (2). In either case, the range of calculated thermobarometric conditions reflected by tschermakite to magnesiohasting-

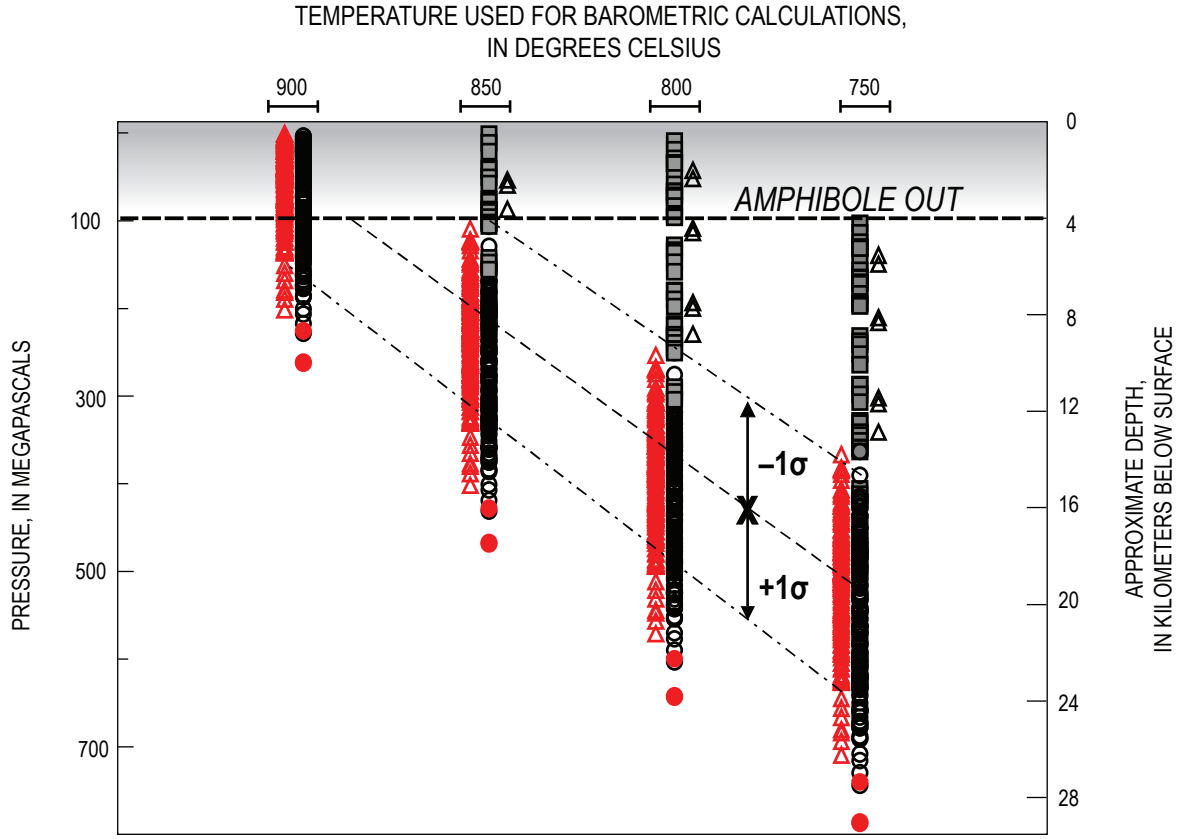

Figure 25. Plot showing results of Al-in-hornblende barometry applied to 2004–6 amphiboles at 750°C, 800°C, 850°C, and 900°C. Symbols correspond to amphibole types, as shown in figure 20. Inferred pressure (depth) versus temperature window for the average (X) and predominant amphibole population (±1σ range) is indicated.

site compositions in new lava reflects a well-mixed population of crystals formed in similar dacite magma over a likely depth range of 4–13.5 km, or possibly as deep as 15 km.

Our calculations suggest that low-Al magnesiohornblendes require low crystallization temperatures (750–850°C) to yield minimum pressures of amphibole stability (>100 MPa, fig. 25). Their presence in the mix suggests entrainment of near-solidus, and perhaps older, dacite mush (along with gabbroic material) in hotter 2004–6 magma. Those low-Al amphiboles that are not xenocrysts may have crystallized at low pressures and temperatures from host dacite melt. The highest Al-tschermakite, magnesiohastingsite, and pargasite could be derived from a mafic source (magma or wall rock) or could have crystallized from dacite under high *P-T* conditions above plagioclase saturation. In either case, magma crystallizing the end-member, high-Al amphiboles may not be close to quartz-saturation or to five-phase saturation conditions. In this case, barometry calculations would yield untenably low pressures over the temperature range of interest.

Amphibole Decompression Reactions, Magma Ascent Dynamics, and Conduit Geometry

The nature and extent of amphibole dissolution and reaction associated with variable decompression paths of dacite magma are documented in the recently published experimental study of Browne and Gardner (2006). Data from their series of isothermal decompression runs, performed on similar compositions and initially equilibrated under conditions analogous to those of the Mount St. Helens 2004–6 magma (840°C and 150 MPa), help to constrain paths of magma ascent. Reaction rims similar to the typical 5-μm rims on subhedral, resorbed, or fragmented amphibole crystals in the 2004–6 Mount St. Helens dacite were reproduced by isothermal decompression from 60 to <30 MPa (~2.5- to <1-km depth) over an interval of 3 to 4 days (compare textures in our fig. 7 with those in fig. 4 of Browne and Gardner, 2006). Such 5-μm rims must have formed by the time magma reached the uppermost conduit because amphibole ceases to react at depths less than ~0.6 km in a highly viscous, nearly solidified, and completely degassed host (Browne and Gardner, 2006).

Textures of resorbed amphibole crystals seen in the 2004–6 Mount St. Helens dacite (fig. 7) could be produced if the host magma stalled for ~2 days at ~3.5 to 2.5-km depth (90 to 60 MPa) during ascent (Browne and Gardner, 2006). Under such conditions, amphibole dissolves without forming pseudomorph reaction rims, which develop subsequent to resorption during further ascent. The disappearance of amphibole, as documented by resorption textures and decreased modal abundance in experimental products, is accompanied by nucleation and growth of orthopyroxene and plagioclase (±Fe-Ti oxide) microphenocrysts in the vicinity of dissolved amphibole. Such microphenocrysts are likely to have contributed to the microcrystalline matrix, which further develops during ascent (Blundy and Cashman, 2001; Cashman and others, this volume, chap. 19).

Amphiboles with <3-μm rims in early dome samples with a glassier matrix (figs. 9*A*, 9*B*; and Pallister and others, this volume, chap. 30) suggest faster ascent rates through the 60–30-MPa pressure range than later dacite, consistent with the relatively high eruptive flux during the earliest phases of dome extrusion (Schilling and others, this volume, chap. 8; Reagan and others, this volume, chap. 37).

The sporadic occurrence of wider reaction rims (30–200 μm) may be attributed to the haphazard entrainment of amphibole phenocrysts subjected to extensive reaction while occluded to walls of the lower conduit. Alternatively, some phenocrysts with wide reaction rims could be xenolithic fragments of 1980s dacite, which is known to have two reaction-rim populations (10–12 and 30 μm; Rutherford and Hill, 1993). Composite phenocrysts with resorbed and patchy cores surrounded by subhedral zoned overgrowths and amphibole-to-amphibole reactions probably reflect xenocryst assimilation at depth. It is evident from less commonly observed examples of resorbed medium-Al amphibole crystals with low-Al (and high fluorine) amphibole overgrowths (for example, in SH314-1 and DRS_3_9_4; fig. 11, table 2) that this style of amphibole dissolution and reaction has occurred in magma stored at depths near to and perhaps slightly above the limits of amphibole stability. Such cases would seem to reflect the disruption of a crystal mush by a hotter or chemically incompatible melt. Rutherford and Devine (this volume, chap. 31) suggest that fluorine has the effect of stabilizing amphibole at depths above that of H_2O-only amphibole saturation. Thus, it is possible that late-stage fluorine enrichment could promote the occurrence of such amphibole-to-amphibole+melt reactions in the lower conduit.

The persistent 5-μm amphibole rims in all post-November 2004 spine lava reflect steady influx and upward transport of magma through the lower conduit, possibly on the order of 2–4 days, from 3.5–2.5-km depths to as shallow as ~1 km. Thus, an amphibole-based rate of magma ascent for this depth interval is between ~600 and ~1,200 m/day. As constrained by a first-year erupted volume of about 70×10^6 m^3 (Schilling and others, this volume, chap. 8), such rates infer a conduit radius between 10 and 5 m. In contrast, ground deformation and eruptive flux infer a significantly larger average conduit radius of ~35 m (down to 5 km depth) (Dzurisin and others, this volume, chap. 14).

A similar discrepancy existed between conduit dimensions inferred from amphibole-rim and volumetric-flux modeling of the 1980s dome-building eruption (Cashman, 1992; Pallister and others, 1992). For the current eruption, both interpretations might be valid, but for different depth ranges. Taken together, these analyses suggest that the conduit may have a wineglass shape. At ~3.5–1-km depth, the conduit might be a narrow pipe (or short dike) that accommodates relatively rapid transit of dacite magma, as recorded by the thin amphibole

reaction rims. Above ~1 km, where matrix crystallization of magma occurs (Cashman and others, this volume, chap. 19; Pallister and others this volume, chap. 30) and amphibole reactions cease, a cooling, solidifying, and sluggishly moving magma is accommodated by a wider conduit (>60 m radius). Such a wineglass shape for the conduit also might help explain (1) the apparent localization of deformation to the crater and to a deep region whose centroid lies at depth of ~8 km (Dzurisin and others, this volume, chap. 14; Lisowski and others, this volume, chap. 15) and (2) the lack of geophysical or petrologic evidence for magma storage between ~4–5-km and ~1-km depths.

The Amphibole Perspective: from Source to Surface

Our study of amphibole systematics shows the near-solid magma recently extruded from Mount St. Helens is a well-blended, crystal-rich dacite mush that originated from depths of at least ~4 km and ascended to within 1 km of the surface at rates in the range ~0.6–1.2 km/day. The compositional ranges of amphibole phenocrysts in the 2004–6 dacite reflect multiple generations of (primarily) dacite magma crystallization in different *P-T* environments. Amphibole morphology and texture reveal a dynamic magma-mixing regime in which a genetically disparate, amphibole phenocryst assemblage is variably dissolved, overgrown, broken, and abraded. The same ranges of amphibole compositions and textures are found in all thin sections of dome material. An obvious implication of the well-dispersed amphibole variability is that the monotonous bulk chemistry of new lava is the result of fine-scale (less than a cubic centimeter) blending of multiple, crystal-laden dacite magmas.

Petrologic constraints, including complex zoning in some amphibole phenocrysts, have spawned models in which this latest generation of Mount St. Helens lava evolved physically and chemically to its preeruptive condition by convective recycling of crystal-laden dacite magma through a contiguous *P-T* regime (such as that depicted in the simplified magma-reservoir diagrams of Pallister and others, this volume, chap. 30, fig. 22; Rutherford and Devine, this volume, chap. 31, fig. 13). Our thermobarometric calculations place amphibole crystallization in a *P-T* window between 100 and ~350–400 MPa (~4- and 13.5–15-km depth) and ~900°C and ~800°C. This interpretation of the *P-T* regime for eruption-related magmatism is within that constrained by experimentally determined phase relations (Rutherford and Devine, this volume, chap 31) and is consistent with the seismologically defined 4–12-km-deep magma source (Moran, 1994).

The broad *P-T* regime reflected in the variety of phenocrysts also could be an artifact of repeated injection of different crystal-laden, dacite magma batches under more restricted *P-T* conditions in the uppermost zone of the magma reservoir. Amphibole petrology and several other lines of evidence suggest that much of the blending of the 2004–6 dacite mush is achieved between ~8- and 4-km depth. The average amphibole in 2004–6 magma is interpreted to have crystallized at 850°C and 220 MPa (fig. 25). Coincidentally, those same source conditions were interpreted for the May 18, 1980, pumice (Rutherford and others, 1985). Considering that the range of amphibole compositions of 2004–6 dacite is comparable to that of amphibole in 1980–86 lava, we suggest a consistent staging area at and above ~8-km depth for both eruptions. Thermobarometric calculations indicate that cyclic variations within the range of the predominant 2004–6 amphibole compositions could result from heating and cooling within this upper part of a magma reservoir (fig. 25). Compositional zoning in the outer parts of plagioclase in the 2004–6 dacite are likewise consistent with injections of hotter, porphyritic dacite magma into crystal-laden dacite mush (Streck and others, this volume, chap. 34).

Isotopic studies of plagioclase in 2004–6 dacite (Cooper and Donnelly, this volume, chap. 36; Kent and others, this volume, chap. 35) suggest that the majority of phenocrysts are "zero-age" and cognate to the host dacite. Of the remaining phenocrysts, a small proportion are Tertiary xenocrysts, but 20–40 percent of analyzed plagioclase crystals are considered antecrysts, derived from prior generations of Mount St. Helens dacite (see Bacon and Lowenstern, 2005, for further discussion of the term, antecryst). Our data indicate that amphibole phenocrysts have a similarly diverse heritage. Although 2004–6 dacite antecrysts may be an inevitable product of long-term mixing, it is also likely that some of them, as well as xenocrysts, are assimilated from variably aged roof rocks and surrounding crustal materials by intrusive processes.

The disequilibrium reflected both in the textural variety of amphiboles and in the wide variation of their outermost rim compositions is a clear indication of a dynamic, preeruptive, magma-mixing environment for the 2004–6 dacite. Uniform reaction rims on all subhedral, rounded, resorbed, and fragmented amphibole phenocrysts of all compositional affinities indicate that this crystal assemblage was being broken, abraded, and dissolved in the magma immediately before and during early stages of ascent. An ascent path that accommodates these features involves differential flow rates through regions of the lowermost conduit and uppermost magma reservoir. In this scenario, supported by experimental observations of Browne and Gardner (2006), some magma must stagnate long enough at 90–60 MPa (~3.5–2.5-km depth) for amphiboles to be resorbed, but other magma does not. This situation seems plausible for a magma ascending through deep conduit roots that must extend into a mushy reservoir cupola. The crystal-laden magma is viscous enough to fragment and entrain additional amphibole phenocrysts during ascent through crystal mushes in the upper reservoir and lower conduit at ~5–3.5 km. Small reaction rims on the well-mixed amphibole assemblage result from rapid decompression of host-dacite magma during ascent through a small conduit (≤10-m radius) extending upward from ~3.5 km to within ~1 km of the crater floor. From ~1 km to the surface, the final

preeruptive condition of amphibole is frozen in as the magma quenches into a nearly solid plug of porphyritic lava. During and after this magma-to-lava transition, a relatively sluggish plug ascent is accommodated by an enlarged (≥60-m radius) uppermost conduit, in which the fresh dacite lava is sheared and gouged during forceful expulsion as lava spines.

Acknowledgments

We thank Jeff Linscott of JL Aviation, whose adept piloting skills enabled heli-dredge collection of lava samples, and Bobbie Myers of the U.S. Geological Survey's Cascades Volcano Observatory (USGS–CVO), who helped to ensure the safety of our dome-sampling forays. Assistance with sample processing and archiving by Winston Stokes (USGS–CVO) and dedicated volunteers in the CVO Petrology Laboratory (Siobhan McConnell, Trystan Herriott, Taryn Lopez, and Alison Eckberg) is gratefully acknowledged. Isabelle Brownfield (USGS, Denver) provided many of the SEM images used in the course of this investigation. Thoughtful reviews of an early version of this chapter by Roz Helz (USGS, emeritus) and Mac Rutherford (Brown University) resulted in significant improvements.

References Cited

Allen, J.C., and Boettcher, A.L., 1978, Amphiboles in andesite and basalt, II—Stability as a function of P-T-f_{H_2O}-f_{O_2}: American Mineralogist, v. 63, nos. 11–12, p. 1074–1087.

Anderson, J.L., and Smith, D.R., 1995, The effects of temperature and f_{O_2} on the Al-in-hornblende barometer: American Mineralogist, v. 80, p. 549–599.

Bachmann, O., and Dungan, M.A., 2002, Temperature-induced Al-zoning in hornblendes of the Fish Canyon magma, Colorado: American Mineralogist, v. 87, p. 1062–1076.

Bacon, C.R., and Lowenstern, J.B., 2005, Late Pleistocene granodiorite source for recycled zircon and phenocrysts in rhyodacite lava at Crater Lake, Oregon: Earth and Planetary Science Letters, v. 233, p. 277–293.

Blundy, J., and Cashman, K., 2001, Ascent-driven crystallisation of dacite magmas at Mount St. Helens, 1980–1986: Contributions to Mineralogy and Petrology, v. 140, no. 6, p. 631–650, doi:10.1007/s004100000219.

Blundy, J.D., and Holland, T.J.B., 1990, Calcic amphibole equilibria and a new plagioclase-amphibole geothermometer: Contributions to Mineralogy and Petrology, v. 104, no. 2, p. 208–224, doi:10.1007/BF00306444.

Browne, B.L., and Gardner, J.E., 2006, The influence of magma ascent path on the texture, mineralogy, and formation of hornblende reaction rims: Earth and Planetary Science Letters, v. 246, p. 161–176.

Buckley, V.J.E., Sparks, R.S.J., and Wood, B.J., 2006, Hornblende dehydration reactions during magma ascent at Soufrière Hills Volcano, Montserrat: Contributions to Mineralogy and Petrology, v. 151, no. 2, p. 121–140, doi:10.1007/s00410-005-0060-5.

Cashman, K.V., 1992, Groundmass crystallization of Mount St, Helens dacite, 1980–1986—a tool for interpreting shallow magmatic processes: Contributions to Mineralogy and Petrology, v. 109, no. 4, p. 431–449, doi:10.1007/BF00306547.

Cashman, K.V., and McConnell, S.M., 2005, Multiple levels of magma storage during the 1980 summer eruptions of Mount St. Helens, WA: Bulletin of Volcanology, v. 68, no. 1, p. 57–75, doi:10.1007/s00445-005-0422-x.

Cashman, K.V., Thornber, C.R., and Pallister, J.S., 2008, From dome to dust; shallow crystallization and fragmentation of conduit magma during the 2004–2006 dome extrusion of Mount St. Helens, Washington, chap. 19 *of* Sherrod, D.R., Scott, W.E., and Stauffer, P.H., eds., A volcano rekindled; the renewed eruption of Mount St. Helens, 2004–2006: U.S. Geological Survey Professional Paper 1750 (this volume).

Cooper, K.M., and Donnelly, C.T., 2008, ^{238}U-^{230}Th-^{226}Ra disequilibria in dacite and plagioclase from the 2004–2005 eruption of Mount St. Helens, chap. 36 *of* Sherrod, D.R., Scott, W.E., and Stauffer, P.H., eds., A volcano rekindled; the renewed eruption of Mount St. Helens, 2004–2006: U.S. Geological Survey Professional Paper 1750 (this volume).

Dzurisin, D., Lisowski, M., Poland, M.P., Sherrod, D.R., and LaHusen, R.G., 2008, Constraints and conundrums posed by ground deformation measurements during the 2004–2006 dome-building eruption of Mount St. Helens, Washington, chap. 14 *of* Sherrod, D.R., Scott, W.E., and Stauffer, P.H., eds., A volcano rekindled; the renewed eruption of Mount St. Helens, 2004–2006: U.S. Geological Survey Professional Paper 1750 (this volume).

Grove, T.L., Elkins-Tanton, L.T., Parman, S.W., Chatterjee, N., Müntener, O., and Gaetani, G.A., 2003, Fractional crystallization and mantle melting controls on calc-alkaline differentiation trends: Contributions to Mineralogy and Petrology, v. 145, p. 515–533.

Hammarstrom, J.M, and Zen, E-an, 1986, Aluminum in hornblende; an empirical igneous geobarometer: American Mineralogist, v. 71, p. 1297–1313.

Hammarstrom, J.M., and Zen, E-an, 1992, Discussion of Blundy and Holland's (1990) "Calcic amphibole equilibria and a new amphibole-plagioclase geothermometer":

Contributions to Mineralogy and Petrology, v. 111, no. 2, p. 264–266, doi:10.1007/BF00348957.

Helz, R.T., 1982, Phase relations and compositions of amphiboles produced in studies of the melting behavior of rocks, *in* Veblen, D.R., and Ribbe, P.H., eds., Amphiboles—petrology and experimental phase relations: Reviews in Mineralogy, v. 9B, p. 279–346.

Holland, T., and Blundy, J., 1994, Non-ideal interactions in calcic amphiboles and their bearing on amphibole-plagioclase thermometry: Contributions to Mineralogy and Petrology, v. 116, no. 4, p. 433–447, doi:10.1007/BF00310910.

Jarosewich, E., Nelen, J.A., and Norberg, J.A., 1980, Reference samples for electron microprobe analyses: Geostandards Newsletter, v. 4, no. 1, p. 43–47.

Johnson, M.C., and Rutherford, M.J., 1989, Experimental calibration of the aluminum-in-hornblende geobarometer with application to Long Valley caldera (California) volcanic rocks: Geology, v. 17, p. 837–841.

Kent, A.J.R., Jacobsen, B., Peate, D.W., Waight, T.E., and Baker, J.A., 2004, Isotope dilution MC-ICP-MS rare earth element analysis of geochemical reference materials NIST SRM 610, NIST SRM 612, NIST SRM 614, BHVO-2G, BHVO-2, BCR-2G, JB-2, WS-1, W-2, AGV-1, AGV-2: Geostandards Newsletter, v. 28, p. 417–430.

Kent, A.J.R., Rowe, M.C., Thornber, C.R., and Pallister, J.S., 2008, Trace element and Pb isotope composition of plagioclase from dome samples from the 2004–2005 eruption of Mount St Helens, Washington, chap. 35 *of* Sherrod, D.R., Scott, W.E., and Stauffer, P.H., eds., A volcano rekindled; the renewed eruption of Mount St. Helens, 2004–2006: U.S. Geological Survey Professional Paper 1750 (this volume).

Leake, B.E., Woolley, A.R., Arps, C.E.S., Birch, W.D., Gilbert, M.C., Grice, J.D., Hawthorne, F.C., Kato, A., Kisch, H.J., Krivovichev, V.G., Linthout, K., Laird, J., Mandarino, J.A., Maresch, W.V., Nickel, E.H., Rock, N.M.S., Schumacher, J.C., Smith, D.C., Stephenson, N.C.N., Ungaretti, L., Whittaker, E.J.W., and Youzhi, G., 1997, Nomenclature of amphiboles—report of the subcommittee on amphiboles of the International Mineralogical Association, Commission on New Minerals and Mineral Names: American Mineralogist, v. 82, nos. 9–10, p. 1019–1037.

Lisowski, M., Dzurisin, D., Denlinger, R.P., and Iwatsubo, E.Y., 2008, GPS-measured deformation associated with the 2004–2006 dome-building eruption of Mount St. Helens, Washington, chap. 15 *of* Sherrod, D.R., Scott, W.E., and Stauffer, P.H., eds., A volcano rekindled; the renewed eruption of Mount St. Helens, 2004–2006: U.S. Geological Survey Professional Paper 1750 (this volume).

Moran, S.C., 1994, Seismicity at Mount St. Helens, 1987–1992; evidence for repressurization of an active magmatic system: Journal of Geophysical Research, v. 99, no. B3, p. 4341–4354, doi:10.1029/93JB02993.

Pallister, J.S., Heliker, C., and Hoblitt, R.P., 1991, Glimpses of the active pluton below Mount St. Helens [abs.]: Eos (American Geophysical Union Transactions), v. 72, no. 44, supplement, p. 576.

Pallister, J.S., Hoblitt, R.P., Crandell, D.R., and Mullineaux, D.R., 1992, Mount St. Helens a decade after the 1980 eruptions—magmatic models, chemical cycles, and a revised hazards assessment: Bulletin of Volcanology, v. 54, no. 2, p. 126–146, doi:10.1007/BF00278003.

Pallister, J.S., Thornber, C.R., Cashman, K.V., Clynne, M.A., Lowers, H.A., Mandeville, C.W., Brownfield, I.K., and Meeker, G.P., 2008, Petrology of the 2004–2006 Mount St. Helens lava dome—implications for magmatic plumbing and eruption triggering, chap. 30 *of* Sherrod, D.R., Scott, W.E., and Stauffer, P.H., eds., A volcano rekindled; the renewed eruption of Mount St. Helens, 2004–2006: U.S. Geological Survey Professional Paper 1750 (this volume).

Pearce, N.J.G., Perkins, W.T., Westgate, J.A., Gorton, M.P., Jackson, S.E., Neal, C.R., and Chenery, S.P., 1997, A compilation of new and published major and trace element data for NIST SRM 610 and NIST SRM 612 glass reference materials: Geostandards Newsletter, v. 21, p. 115–144.

Pichavant, M., Valencia, H.J., Boulmier, S., Briqueu, L., Joron, J., Juteau, M., Marin, L., Michard, A., Sheppard, S.M.F., Treuil, M., and Vernet, M., 1987, The Macusani glasses, SE Peru; evidence of chemical fractionation in peraluminous magmas, *in* Mysen, B.O., ed., Magmatic processes—physiochemical principles: Geochemical Society Special Publication No. 1, p. 359–373.

Reagan, M.K., Cooper, K.M., Pallister, J.S., Thornber, C.R., and Wortel, M., 2008, Timing of degassing and plagioclase growth in lavas erupted from Mount St. Helens, 2004–2005, from ^{210}Po-^{210}Pb-^{226}Ra disequilibria, chap. 37 *of* Sherrod, D.R., Scott, W.E., and Stauffer, P.H., eds., A volcano rekindled; the renewed eruption of Mount St. Helens, 2004–2006: U.S. Geological Survey Professional Paper 1750 (this volume).

Rowe, M.C., Thornber, C.R., Gooding, D.J., and Pallister, J.S., 2008, Catalog of Mount St. Helens 2004–2005 tephra samples with major- and trace-element geochemistry: U.S. Geological Survey Open-File Report 2008–1131, 7 p, with digital database.

Rutherford, M.J., and Devine, J.D., III, 2008, Magmatic conditions and processes in the storage zone of the 2004–2006 Mount St. Helens dacite, chap. 31 *of* Sherrod, D.R., Scott, W.E., and Stauffer, P.H., eds., A volcano rekindled; the renewed eruption of Mount St. Helens, 2004–2006: U.S. Geological Survey Professional Paper 1750 (this volume).

Rutherford, M.J., and Hill, P.M., 1993, Magma ascent rates from amphibole breakdown—an experimental study applied to the 1980–1986 Mount St. Helens eruptions: Journal of Geophysical Research, v. 98, no. B11, p. 19667–19685.

Rutherford, M.J., and Johnson, M.C., 1992, Comment on Blundy and Holland's (1990) "Calcic amphibole equilibria and a new amphibole-plagioclase geothermometer": Contributions to Mineralogy and Petrology, v. 111, no. 2, p. 266–268.

Rutherford, M.J., Sigurdsson, H., Carey, S., and Davis, A., 1985, The May 18, 1980, eruption of Mount St. Helens; 1. melt composition and experimental phase equilibria: Journal of Geophysical Research, v. 90, no. B4, p. 2929–2947.

Schilling, S.P., Thompson, R.A., Messerich, J.A., and Iwatsubo, E.Y., 2008, Use of digital aerophotogrammetry to determine rates of lava dome growth, Mount St. Helens, 2004–2005, chap. 8 *of* Sherrod, D.R., Scott, W.E., and Stauffer, P.H., eds., A volcano rekindled; the renewed eruption of Mount St. Helens, 2004–2006: U.S. Geological Survey Professional Paper 1750 (this volume).

Streck, M.J., Broderick, C.A., Thornber, C.R., Clynne, M.A., and Pallister, J.S., 2008, Plagioclase populations and zoning in dacite of the 2004–2005 Mount St. Helens eruption—constraints for magma origin and dynamics, chap. 34 *of* Sherrod, D.R., Scott, W.E., and Stauffer, P.H., eds., A volcano rekindled; the renewed eruption of Mount St. Helens, 2004–2006: U.S. Geological Survey Professional Paper 1750 (this volume).

Sun, S.-s., and McDonough, W.F., 1989, Chemical and isotopic systematics of oceanic basalts—implications for mantle composition and processes, *in* Saunders, A.D., and Norry, M.J., eds., Magmatism in the ocean basins: Geological Society of London Special Publications 42, p. 313–345.

Thornber, C.R., Pallister, J.S., Rowe, M.C., McConnell, S., Herriott, T.M., Eckberg, A., Stokes, W.C., Johnson Cornelius, D., Conrey, R.M., Hannah, T., Taggart, J.E., Jr., Adams, M., Lamothe, P.J., Budahn, J.R., and Knaack, C.M., 2008, Catalog of Mount St. Helens 2004–2007 dome samples with major- and trace-element chemistry: U.S. Geological Survey Open-File Report 2008–1130, 9 p., with digital database.

Appendix 1. Analytical Methods

Microbeam analyses and imagery used in this study were accomplished at three different laboratories. Most data were obtained using the USGS Denver JEOL 8900 electron microprobe and a JEOL 5800-LV scanning electron microscope (SEM). Nine samples were analyzed and imaged by M. Rowe at Oregon State University on a Cameca SX-100 electron microprobe. At both laboratories, amphibole grains were analyzed using 20-nA beam current and a 15 keV accelerating voltage. For all but the smallest of grains, which required a fully focused beam, a 10-µm beam diameter was used for crystal interiors and near-rim analyses. Count times for major elements varied between 30 and 10 s on peak (15 to 5 s background count times). For F and Cl, count times on peak were increased to 60 and 40 s, respectively. USNM natural silicate mineral standards were used for calibration. Kakanui hornblende (Jarosewich and others, 1980) was repeatedly analyzed to monitor accuracy and precision during and among runs.

Additional analyses of SH304-2A (early dacite) and SH304-2G (glassy lithic fragment) amphibole crystals were done by C. Mandeville at the American Museum of Natural History (AMNH) using a Cameca SX-100 electron microprobe utilizing a 15-keV accelerating voltage, 10-nA beam current for major elements, 15-µm beam diameter, 30 s count time on peak and 15 s on background. F, Cl, and Cr analyses of amphiboles by electron microprobe at AMNH were done during the same analytical session with 15-keV accelerating voltage, 40-nA beam current, and 140 s count time on peak and 70 s on background. Precision and accuracy of major-element analyses were checked by repeated analyses of Kakanui hornblende. Precision and accuracy of F, Cl, and Cr analyses at AMNH were monitored by repeated analyses of Macusani peraluminous rhyolite glass (1.3 percent F, 450 ppm Cl; Pichavant and others, 1987), NMNH 164905 chromium-augite (0.85 percent Cr; Jarosewich and others, 1980), and NIST SRM 610 glass (415±49.5 ppm Cr; Pearce and others, 1997).

All amphibole analyses used in this investigation fit the mineralogical criteria established for clinoamphiboles by Leake and others (1997). See text for discussion of the stoichiometric calculation used to assess cation site occupancy and proper nomenclature.

Trace-element concentrations of amphiboles were analyzed by laser ablation inductively coupled plasma mass spectrometry (LA ICP-MS) in the W.M. Keck Collaboratory for Plasma Spectrometry, Oregon State University, and collected from the same phenocryst areas that were analyzed and imaged by the Cameca SX-100 electron microprobe. Amphiboles were ablated with a NuWave 213 nm Nd:YAG laser using a 40-µm stationary spot and 20-Hz pulse rate. Ablation time and data acquisition for each analysis was 30 s, with 45 s of washout time before and after ablation. Measured counts were normalized to ^{43}Ca. Trace-element concentrations were then calculated relative to the BCR-2G glass standard. BHVO-2G glass standard was ablated under identical conditions as the amphiboles as a secondary standard. Precision, estimated by repeated analysis of BHVO-2G, is within 10 percent of reported values for all trace elements (Kent and others, 2004).

Appendix 2. Major- and Trace-Element Compositions of Amphibole Phenocrysts in Mount St. Helens 2004–2006 and 1980–1986 Dacite Lava

[This appendix appears only in the digital versions of this work—in the DVD-ROM that accompanies the printed volume and as a separate file accompanying this chapter on the Web at: http://pubs.usgs.gov/pp/1750.]

The Mount St. Helens amphibole phenocryst chemistry described in this chapter is tabulated in six worksheets of a Microsoft Excel file. The six worksheets are organized as follows:

Worksheet 1. Electron microprobe analyses of amphibole phenocrysts in Mount St. Helens 2004–6 dacite.
Worksheet 2. Electron microprobe analyses of amphibole phenocrysts in Mount St. Helens 2004 glassy lithic fragments.
Worksheet 3. Electron microprobe analyses of amphibole phenocrysts in Mount St. Helens 2004–6 lithic inclusions.
Worksheet 4. Electron microprobe analyses of amphibole phenocryst cores in Mount St. Helens 1986 gabbro xenoliths.
Worksheet 5. Electron microprobe analyses of amphibole phenocryst cores in Mount St. Helens 1980–86 dacite.
Worksheet 6. LA-ICPMS rare-earth-element analyses of amphibole phenocrysts in Mount St. Helens 2004–6 dacite.